Methane Generation from CO_2 with a Molecular Rhenium Catalyst

John K. Nganga,[1] Lucienna M. Wolf,[2] Kankana Mullick,[1] Eric Reinheimer,[3] Cesar Saucedo,[2] Megan E. Wilson,[2] Kyle A. Grice,[2,*] Mehmed Z. Ertem,[4,*] and Alfredo M. Angeles-Boza[1,5,*]

[1] *Department of Chemistry, University of Connecticut, Storrs, Connecticut 06269-30602*

[2] *Department of Chemistry and Biochemistry, DePaul University, Chicago, Illinois 60614*

[3] *Rigaku, 9009 New Trails Drive, The Woodlands, Texas 77381*

[4] *Chemistry Division, Energy & Photon Sciences Directorate, Brookhaven National Laboratory, Bldg. 555A, Upton, New York 11973*

[5] *Institute of Materials Science, University of Connecticut, Storrs, Connecticut 06269-3060*

*E-mail for K.A.G.: kgrice1@depaul.edu.

*E-mail for M.Z.E.: mzertem@bnl.gov.

*E-mail for A.M.A.-B.: alfredo.angeles-boza@uconn.edu.

Abstract: The atomic level tunability of molecular structures is a compelling reason to develop homogeneous catalysts for challenging reactions such as the electrochemical reduction of carbon dioxide to valuable C_1-C_n products. Of particular interest is methane, the largest component of natural gas. Herein, we report a series of three isomeric rhenium tricarbonyl complexes coordinated by the asymmetric diimine ligands 2-(isoquinolin-1-yl)-4,5-dihydrooxazole (**quin-1-oxa**), 2-(quinolin-2-yl)-4,5-dihydrooxazole (**quin-2-oxa**), and 2-(isoquinolin-3-yl)-4,5-dihydrooxazole (**quin-3-oxa**) that catalyze the reduction of CO_2 to carbon monoxide and methane, albeit the latter with a low efficiency. To our knowledge, these complexes are the first examples of rhenium(I) catalysts capable of converting carbon dioxide into methane. Re(quin-1-oxa)$(CO)_3$Cl (**1**), Re(quin-2-oxa)$(CO)_3$Cl (**2**) and Re(quin-3-oxa)$(CO)_3$Cl (**3**) were characterized and studied using a variety of electrochemical and spectroscopic techniques. In bulk electrolysis experiments, the three complexes reduce CO_2 to CO and CH_4. When the controlled-potential electrolysis experiments are performed at –2.5 V (vs $Fc^{+/0}$) and in the presence of the Brønsted acid 2,2,2-trifluoroethanol, methane is produced with turnover numbers that range from 1.3 to 1.8. Isotope labelling experiments using $^{13}CO_2$ atmosphere produce $^{13}CH_4$ (m/z = 17) confirming that methane originates from CO_2 reduction. Theoretical calculations are performed to investigate the mechanistic aspects of the $8e^-/8H^+$ reduction of CO_2 to CH_4. A ligand assisted pathway is proposed to be an efficient pathway in formation of CH_4. Delocalization of the electron density on the (iso)quinoline moiety upon reduction stabilizes the key carbonyl intermediate leading to additional reactivity of this ligand. These results should aid the development of more robust catalytic systems that produce CH_4 from CO_2.

Introduction

Climate change and its consequences, such as ocean acidification and the accelerated rise of the global mean sea level, are associated with carbon dioxide (CO_2) emissions from human activity.[1] Atmospheric carbon dioxide has surpassed 400 parts per million (ppm) and levels are the highest values since records began. Considerable effort has been directed toward climate change mitigation by developing new pathways for chemical fixation of CO_2.[2-12] Particularly interesting are the processes that recycle CO_2 into useful chemicals.[3-5] For example, renewable solar energy could be used to produce hydrocarbon fuels, such as methane, from CO_2. Products such as CO, formic acid, or alcohols are also desirable.[10] However, these products require multi-electron/multi-proton reactions that are often in competition with hydrogen production and therefore catalysts must be developed to control CO_2 reduction selectivity and activity.

Transition metal catalysts have been investigated extensively for their CO_2 reduction activity.[13-18] Metal catalysts can enable the reduction of the thermodynamically and kinetically stable CO_2 molecule through coordination and activation. Aresta and coworkers isolated the first example of metal-CO_2 complex, in which a CO_2 was coordinated to a nickel complex.[19] Transition metal catalysts not only coordinate CO_2, but are also capable of transferring multiple electrons, avoiding the high energy CO_2 anion radical intermediate. For example, iron porphyrins are efficient CO-selective CO_2 reduction catalysts.[20-21] Besides metallated porphyrins, a number of catalysts that transform CO_2 to CO and other products have been reported.[14] These complexes realize multielectron reactions thanks to the presence of ligands that serve as electron reservoirs. The seminal work of Lehn et al. first showed $Re(bpy)(CO)_3Cl$ (bpy =2,2′-bipyridine) to be an effective catalyst for CO_2 reduction,[22-25] from which an extensive derivatized library of homogeneous photo- and electro-catalysts were built upon, providing valuable insights on

mechanisms by which CO_2 can be activated.[26-34] While rhenium (I) diimine catalysts are among the most studied transition metal catalysts for CO_2 reduction, improvements to their design are still needed to create more effective systems for reduction of CO_2 past the 2-electron product of CO.

We recently examined the use of rhenium complexes containing pyridine-oxazoline ligands as a new family of CO_2 reduction catalyst as these diimine ligands are stable to reducing conditions, easily prepared, and offer great potential for derivatization in multiple sites. In addition, metal complexes of pyridine-oxazoline ligands have demonstrated to be efficient catalysts in a range of catalytic reactions.[35] The complex Re(2-(pyridin-2-yl)-4,5-dihydrooxazole)$(CO)_3Cl$ (**I**) is an active electrocatalyst for CO_2 reduction, with a relative turnover frequency (TOF), $(i_{cat}/i_p)^2$, 5.5 times that of Re(bpy)$(CO)_3Cl$. Interestingly, the electrocatalytic activity of **I** and its derivatives showed an unusual dependence on the donor number (DN) of the solvent.[36]

The long term objective of our program is to rationally design pyridine-oxazoline ligands with multifunctional properties (*e.g.* proton responsive groups, Lewis acids or pendant bases in the second coordination sphere, etc.) that can assist in the metal-based CO_2 reduction catalysis and generate desirable products. However, the electronic properties of the parent system are still not fully understood and minor modifications have drastic effects on catalysis. Herein we report the effects of fusing a benzene ring onto the pyridine on the CO_2 reduction activities of **I** (Figure 1). The quinoline and isoquinoline moieties are hypothesized to provide effective storage of additional redox equivalents needed for CO_2 reduction and the introduction of these moieties allows the study of the effects of heterocyclic units that are more basic (isoquinoline, pK_a = 5.46) or less basic (quinoline, pK_a 4.85) than pyridine (pK_a = 5.22). Through our combined

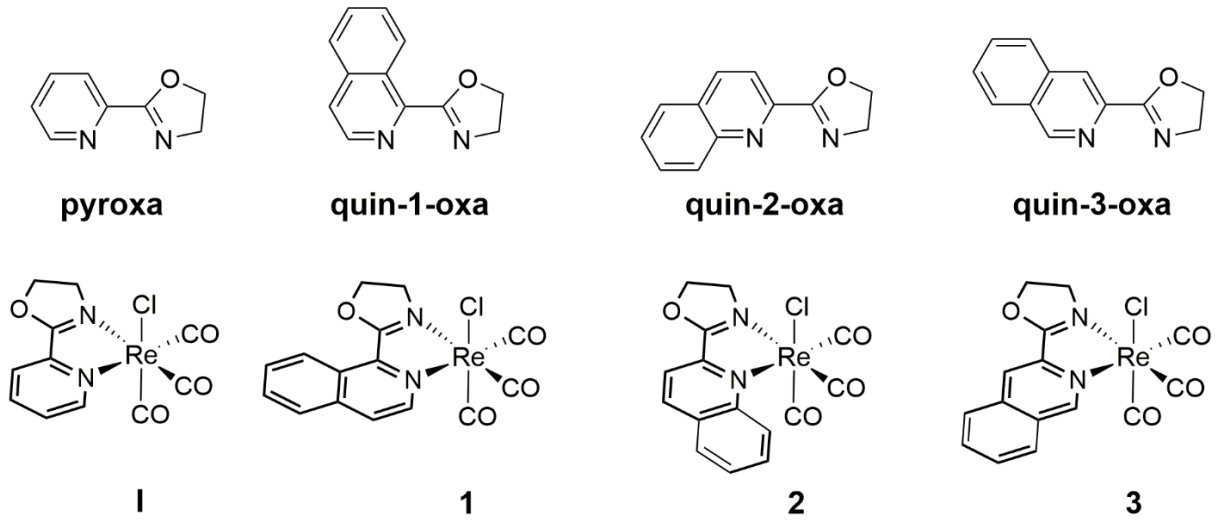

Figure 1. Structural representation of the ligands 2-(isoquinolin-1-yl)-4,5-dihydrooxazole (**quin-1-oxa**), 2-(quinolin-2-yl)-4,5-dihydrooxazole (**quin-2-oxa**), and 2-(isoquinolin-3-yl)-4,5-dihydrooxazole (**quin-3-oxa**) and their rhenium(I) complexes **1**-**3**.

experimental and theoretical study, we present our results on the synthesis and characterization of complexes **1**-**3**, and their ability to catalyze the electrochemical reduction of CO_2 to CO and all the way to the 8-electron product CH_4. To our knowledge, compounds **1**-**3** are the first examples of rhenium-based catalysts to produce CH_4 from CO_2. Based on collective results from spectroscopy, electrochemistry, and theoretical calculations, we discuss the plausible reaction pathways by which these complexes perform the $2e^-/2H^+$ reduction of CO_2 to CO and $8e^-/8H^+$ reduction of CO_2 to CH_4, and the effect of ligand modification on catalysis. Although these complexes yield methane with low efficiencies, we believe that the insight provided by these studies will have significant implications for the design of more efficacious molecular catalysts for the multielectron reduction of CO_2.

Experimental

Materials. Toluene, isobutyl chloroformate, 2-chloroethylamine hydrochloride, potassium hydroxide, magnesium sulfate, 2-quinolinecarboxylic acid, 3-isoquinolinecarboxylic acid,

isoquinoline-1-carboxylic acid, pentacarbonylchlororhenium(I) were purchased from Sigma Aldrich. Sodium chloride and ammonium chloride were purchased from J.T. Baker. Methanol, dichloromethane and triethylamine were purchased from Fisher Scientific. For cyclic voltammetry the solvents acetonitrile, dimethylformamide (DMF) and dimethyl sulfoxide (DMSO) were obtained from the Pure Process technology (PPT) Free Standing solvent purification system (SPS). The electrochemical grade $[^nBu_4N]PF_6 \geq 99.0\%$ used was purchased from Sigma Aldrich. $[^nBu_4N]Cl$ was purchased from Acros Organics, recrystallized from HPLC-grade ethanol and dried for 48 hours in a vacuum oven before electrochemical analysis.

Syntheses. The synthesis of the ligands 2-(isoquinolin-1-yl)-4,5-dihydrooxazole (**quin-1-oxa**), 2- (quinolin-2-yl)-4,5-dihydrooxazole (**quin-2-oxa**) and 2-(isoquinolin-3-yl)-4,5-dihydrooxazole (**quin-3-oxa)** was achieved according to a previously reported procedure.[37] The ligands were characterized by ^{1}H NMR (Figure S1-3).

*fac-Re(quin-1-oxa)(CO)$_3$Cl (**1**)*. In a 50 mL round-bottom flask, $Re(CO)_5Cl$ (0.2 g, 0.6 mmol), **quin-1-oxa** (0.11 g, 0.6 mol) and toluene (30 mL) were added together, and the reaction mixture was heated to reflux. After 2.5 h, the reaction was allowed to cool down, and the solvent was evaporated under reduced pressure to afford a brown solid (0.23 g, yield = 83%). ^{1}H NMR, (δ, 400 MHz, DMSO-*d*$_6$): 8.95. (dt, 1H), 8.91 (d, 1H), 8.38(m, 1H), 8.04 (dddd, 2H), 5.16(m, 2H), 4.39(m, 1H) 4.18(m, 1H). Elem. Anal. Calcd. for $ReC_{15}H_{10}N_2O_4$: C, 35.75; H, 2.00; N, 5.56. Found: C, 35.86; H, 1.91.; N, 5.65.

*fac-Re(quin-2-oxa)(CO)$_3$Cl (**2**)*. In a 50 mL round-bottom flask, $Re(CO)_5Cl$ (0.2 g, 0.6 mmol), **quin-2-oxa** (0.11 g, 0.6 mol) and toluene (30 mL) were added together, and the reaction mixture was heated to reflux. After 2.5 h, the reaction was allowed to cool down, and the solvent was evaporated under reduced pressure to afford a red solid (0.24 g, yield = 86%). ^{1}H NMR, (δ, 400

MHz, DMSO-d_6): 9.03. (d, 1H), 8.65 (dd, 1H), 8.36(dd, 1H), 8.22 (m, 2H), 7.99 (ddd, 1H), 5.08(td, 2H), 4.47(m, 1H) 4.24(m, 1H). Elem. Anal. Calcd. for $ReC_{15}H_{10}N_2O_4$: C, 35.75; H, 2.00; N, 5.56. Found: C, 35.73; H, 1.87; N, 5.58.

fac-Re(quin-3-oxa)(CO)$_3$Cl ***(3)***. In a 50 mL round-bottom flask, $Re(CO)_5Cl$ (0.2 g, 0.6 mmol), **quin-3-oxa** (0.11 g, 0.6 mol) and toluene (30 mL) were added together, and the reaction mixture was heated to reflux. After 2.5 h, the reaction was allowed to cool down and the solvent was evaporated under reduced pressure to afford a yellow solid (0.22 g, yield = 79%). ^{1}H NMR, (δ, 400 MHz, DMSO-d_6): 9.88. (s, 1H), 8.78 (s, 1H), 8.60(s, 1H), 8.36 (d, 1H), 8.13 (ddd, 1H), 8.05 (d, 1H), 5.04(td, 2H), 4.34(ddd, 1H) 4.16(m, 1H).,^{13}C NMR (δ, 100 MHz, DMSO-d_6). Elem. Anal. Calcd. for $ReC_{15}H_{10}N_2O_4 \bullet 1/3C_7H_8$ C, 38.99; H, 2.40; N, 5.28. Found: C, 38.87; H, 2.38; N 5.24.

Methods. ^{1}H and ^{13}C NMR spectra were recorded on a Bruker AVANCE (300 MHz) or Bruker AVANCE III (400 MHz) system at ambient temperature and were referenced to residual solvent peaks. UV-Vis spectra were recorded on a Cary 50 spectrophotometer. Solution IR spectra (CH_3CN) were carried on a Jasco FT/IR-6100 spectrometer. Elemental analyses were performed at Atlantic Microlab, Inc., in Norcross, GA.

Electrochemistry. Electrochemical experiments were performed by using a Model 6012D Electrochemical analyzer from CH Instruments, Inc. or DY2311 Potentiostat from Digi-Ivy. Cyclic voltammetry experiments were performed under N_2 or CO_2 in a one-compartment cell with a glassy carbon working electrode, a platinum wire counter electrode and a Ag/Ag^+ (10 mM $AgNO_3$ in acetonitrile, DMF or DMSO) reference electrode with ferrocene as an external reference. All experiments were performed with solutions containing 0.1 M tetrabutylammonium hexafluorophosphate ($[^nBu_4N]PF_6$) as the supporting electrolyte, acetonitrile, DMSO or DMF as

the solvent, and rhenium complexes at a concentration of 1.0 mM. Infrared Spectroelectrochemistry (IR-SEC) was performed with a commercially available Optically Transparent Thin Layer Electrochemical (OTTLE) cell purchased from Frantisek Hartl at the University of Reading.[38] The air-tight demountable cell was composed of CaF_2 windows and a Teflon spacer (ca. 0.2 mm optical path). The working electrode was a platinum mini-grid in the path of the IR beam, the counter electrode was a platinum mini-grid, and a silver wire was the pseudoreference. For IR-SEC, HPLC-grade acetonitrile was purified using an Innovative PureSolve system under N_2, and $[^nBu_4N]PF_6$ was purified by recrystallization from HPLC-grade methanol and dried in a vacuum oven overnight. An eDaq ER466 potentiostat was used to apply increasingly negative potentials, and IR spectra were collected with an ABB FLTA2000 IR spectrometer. Samples were dissolved in 0.1 M TBAH/acetonitrile and sparged with argon for 20 minutes prior to analysis.

X-ray Crystallography. Recrystallization of **1-3** from acetonitrile and methanol afforded material suitable for single crystal X-ray crystallography. Red-orange crystals of **1-3** having dimensions 0.28 x 0.25 x 0.13 mm^3 (**1**), 0.10 x 0.09 x 0.07 mm^3 (**2**) and 0.12 x 0.09 x 0.05 mm^3 (**3**) respectively were secured to Mitegen micromounts using Paratone oil, and their single crystal X-ray diffraction data was collected at 100 K using a Rigaku Oxford Diffraction (ROD) Synergy-S X-ray diffractometer equipped with a HyPix-6000HE hybrid photon counting (HPC) detector. For samples **1** and **3**, reflection data were collected using microfocused Mo $K_{\alpha 1}$ radiation (= 0.71073 Å), while microfocused Cu $K_{\alpha 1}$ radiation (= 1.54184 Å) was utilized for **2**. For all samples, data collection strategies to ensure desired completeness and redundancy were determined via CrysAlis^{Pro}.[39] Data processing was done using CrysAlis^{Pro} and included numerical absorption corrections on all samples applied after face-indexing using the SCALE3

ABSPACK scaling algorithm.[40] All structures were solved via intrinsic phasing methods using ShelXT[41] and refined using ShelXL[42] in the Olex2 graphical user interface. Space groups were unambiguously verified by PLATON. The final structural refinements on samples included anisotropic temperature factors on all non-hydrogen atoms. Hydrogen atoms for **1** were attached via the riding model at calculated positions using suitable HFIX commands. The hydrogen atoms in **2** were located in the difference map and refined while those in **3** were introduced using a combination of calculated positions or were located in the difference map. Crystallographic data for the structures in this paper has been deposited with the Cambridge Crystallographic Data Centre with the CCDC numbers 1849894 - 1849896. These data can be obtained free of charge from the Cambridge Crystallographic Data Centre via www.ccdc.cam.ac.uk/data_request/cif.

Computational Methods. All geometries were fully optimized at the M06 level of density functional theory[43] with the SMD continuum solvation model[44] for acetonitrile as solvent using the Stuttgart [8s7p6d2f | 6s5p3d2f] ECP28MWB contracted pseudopotential basis set[45] on Re and the 6-31G(d) basis set on all other atoms.[46] Non-analytical integrals were evaluated using the integral=grid=ultrafine option as implemented in the Gaussian 09 software package.[47] The nature of all stationary points was verified by analytic computation of vibrational frequencies, which were also used for the computation of zero-point vibrational energies, molecular partition functions, and for determining the reactants and products associated with each transition-state structure (by following the normal modes associated with imaginary frequencies). Partition functions were used in the computation of 298 K thermal contributions to the free energy employing the usual ideal-gas, rigid-rotator, harmonic oscillator approximation.[48] Free-energy contributions were added to single-point, SMD-solvated M06 electronic energies computed at the optimized geometries obtained with the initial basis with the SDD basis set on Re and the

larger 6-311+G(2df,p) basis set on all other atoms to arrive at final, composite free energies. The free energy of solvation of proton in acetonitrile is taken as –260.2 kcal/mol.[49]

Standard reduction potentials were calculated for various possible redox couples to assess the energetic accessibility of different intermediates at various oxidation states. For a redox reaction of the form

$$O_{(soln)} + ne^-_{(g)} \rightarrow R_{(soln)} \quad (1)$$

where *O* and *R* denote the oxidized and reduced states of the redox couple, respectively, and *n* is the number of electrons involved in redox reaction, the reduction potential $E^o_{O|R}$ relative to SCE was computed as

$$E^0_{O|R} = -\frac{\Delta G^o_{O|R}}{nF} - \Delta E^o_{ref} \quad (2)$$

where $\Delta G^o_{O|R}$ is the free energy change associated with eq. 1 (using Boltzmann statistics for the electron) and ΔE^o_{ref} is taken as 0.141 V,[50] which is required for the conversion of calculated $E^0_{O|R}$ versus normal hydrogen electrode (NHE) in aqueous solution (E_{NHE}= –4.281 V)[51] to $E^0_{O|R}$ versus the saturated calomel electrode (SCE) in acetonitrile (E_{SCE} = –4.422 V).[52] We obtained reduction potentials referenced to the ferricenium/ferrocene couple by using a shift of –0.384 V from $E^0_{O|R}$ vs SCE.

Results

Synthesis and Characterization of the Re(I) Complexes

The synthesis of the new complexes was carried out by treating $Re(CO)_5Cl$ with the corresponding ligand in refluxing toluene under N_2 for 2.5 hours. The crude products were collected by filtration to provide the Re(I) complexes in good yields (70-80%). Complexes **1-3**

were characterized by ^{1}H and ^{13}C NMR, mass spectrometry, and elemental analysis (see Supporting Information).

Although at first sight, compounds **1-3** are similar to each other, the spectroscopic characterization shows a different picture (Figure 3).[36, 53] The MLCT bands for compounds **1** and **2** appear at 414 nm (ε = 3900 M^{-1} cm^{-1}) and 406 nm (ε = 3300 M^{-1} cm^{-1}), respectively; whereas the MLCT transition of **3** is found at higher energies (shoulder at ~365 nm, $\varepsilon \approx$ 3900 M^{-1} cm^{-1}). When compared to the MLCT band in **I** (λ_{max} = 369, ε = 1400 M^{-1} cm^{-1} in acetonitrile), the MLCT transitions for **1** and **2** appear at longer wavelengths as expected since the **quin-1-oxa**, and **quin-2-oxa** ligands should have π^* orbitals at lower energies as compared to those of the pyridine-oxazoline ligands. In contrast, the band corresponding to the MLCT transition of complex **3** is observed at roughly the same wavelength as that of Re(pyridine-oxazoline)$(CO)_3Cl$

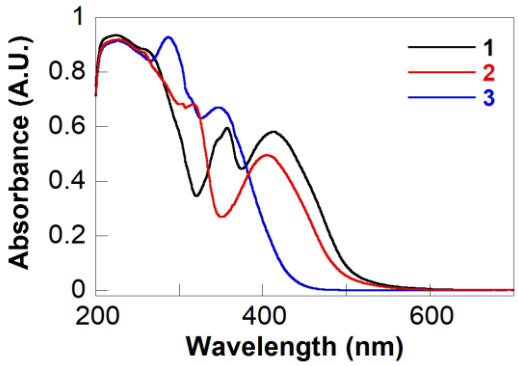

Figure 2. UV-visible absorption spectra of the rhenium(I) complexes **1-3** in acetonitrile at 293 K.

(**I**).

A comparison of the structures obtained by single crystal X-ray diffraction provides additional information about the differences between the three complexes. Crystals of **1** and **2**, suitable for X-ray crystallography were grown from solutions of the complexes in a solution of

1:1 v/v acetonitrile methanol mixture through slow evaporation at room temperature over a period of 5 days. Remarkably, attempted crystallization of **3** resulted in an iminoester derivative

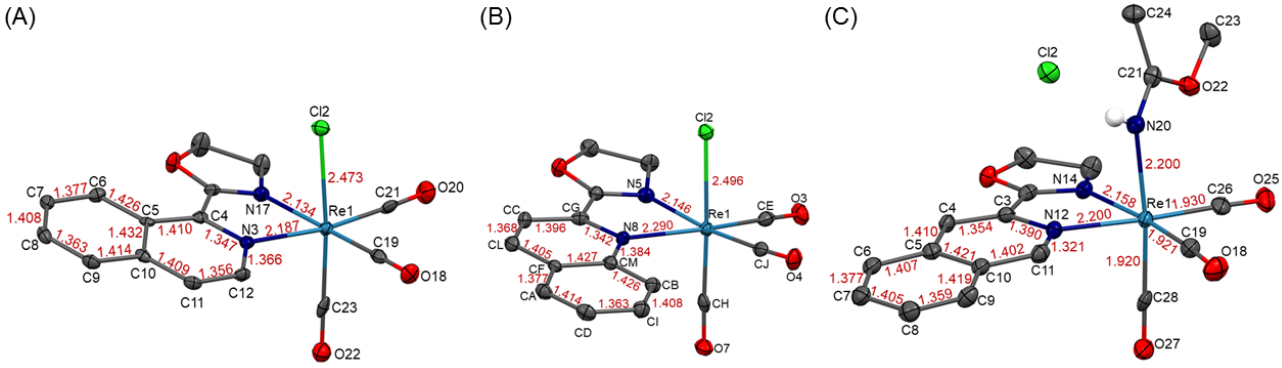

Figure 3. Thermal ellipsoid plots of (A) **1**, (B) **2**, and (C) **3a** at 50% probability. Selected hydrogen atoms are omitted for clarity.

of **3**, **3a** [Re(quin-3-oxa)$(CO)_3$(NHC$(OCH_3)CH_3$)]Cl. Thermal ellipsoid plots of the three compounds are provided in Figures 3A-C. The three structures can be considered as distorted octahedral with three CO groups coordinated in a facial arrangement. The Re-$N_{diimine}$ distances range from 2.134(1) to 2.290(4) Å and resemble those of other rhenium-diimine complexes including the rhenium complexes with pyridine-oxazoline ligands we recently reported.

Complex **2** shows a Re-$N_{quinoline}$ distance that is longer than those observed for the other two complexes or the previously reported Re-$N_{pyridine}$ distance from the rhenium pyridine-oxazoline complexes. This elongation prevents the hydrogen atom on the carbon labeled as CB from colliding with one of the carbonyl ligands. Along with the increased distance between the rhenium atom and, the quinoline moiety in **2**, we determined a larger angle, 104.8(1)°, formed by the $N_{quinoline}$, rhenium atom and the carbon in the carbonyl ligand trans to the oxazoline ring. The angles for complexes **1** and **3a** were 100.3(1)° and 97.4(1)°, respectively. The Re-Cl distances for complexes **1** and **2** are 2.473(1) Å and 2.496(1), respectively, and are similar to previously

reported Re-Cl distances in similar complexes.[36] In **3a** the Cl anion is no longer coordinated but is found to hydrogen-bond the N-H on iminoester ligand that originated from the solvent molecules. The complex **3a** is reminiscent of the iminoester $[Re(bpy)(CO)_3(HN{=}C(CH_3)OCH_2CH_3)](PF_6)$ (**II**) reported by Ishitani and coworkers.[54] The Re-$N_{iminoester}$ distance in **3a** is 2.186(3) Å, similar to that of **II**, 2.178(5) Å, and likewise, the $N_{iminoester}$-C distance are 1.284(4) Å and 1.272(8) Å for **3a** and **II**, respectively.

Electrochemical Studies

Representative voltammograms of solutions of the ligands under an atmosphere of N_2 are shown in Figure 4A. All scans were recorded under nitrogen saturation in dry acetonitrile with 0.1 M tetrabutylammonium hexafluorophosphate ($[^nBu_4N]PF_6$) supporting electrolyte. Ligands **quin-1-oxa**, and **quin-2-oxa** are reduced at –2.29 V and –2.33 V vs $Fc^{+/0}$, respectively; whereas the reduction of **quin-3-oxa** happens at a more negative potential, –2.54 V, than the other two isomers. For complexes **1** and **2**, the first reduction under N_2 atmosphere occur at similar $E_{1/2}$ values, –1.47 V and –1.49 V vs $Fc^{+/0}$, respectively. When the electrolyte is $[^nBu_4N]PF_6$, the i_a/i_c value for the first reduction of **1** and **2** increases with the scan rate from ~0.6 to ~0.8 at 1 V/s. A similar increase in the i_a/i_c ratio is also observed when the electrolyte is $[^nBu_4N]Cl$ at 0.1 V/s (Figure S11). These potentials are ~0.25 V more positive than those found for the first reduction of $Re(pyroxa)(CO)_3Cl$ (**I**).[36] For **1** and **2**, the first quasireversible reduction is ligand based, with the added electron residing on the quinoline or isoquinoline moieties to give $[Re^I(quin\text{-}n\text{-}oxa^{\bullet-})(CO)_3Cl]^-$ (n = 1 or 2), followed by Cl^- dissociation. A second reduction happens at –1.93 V and –1.95 V vs $Fc^{+/0}$, for **1** and **2**, respectively and the additional electron leads to formation of $[Re(quin\text{-}n\text{-}oxa)(CO)_3]^-$. The return scans show the oxidation of the solvato and chloro species at ~-1.29 V and -1.42 V vs $Fc^{+/0}$, respectively (Figure S11-S12). The anodic scan of **2** shows an

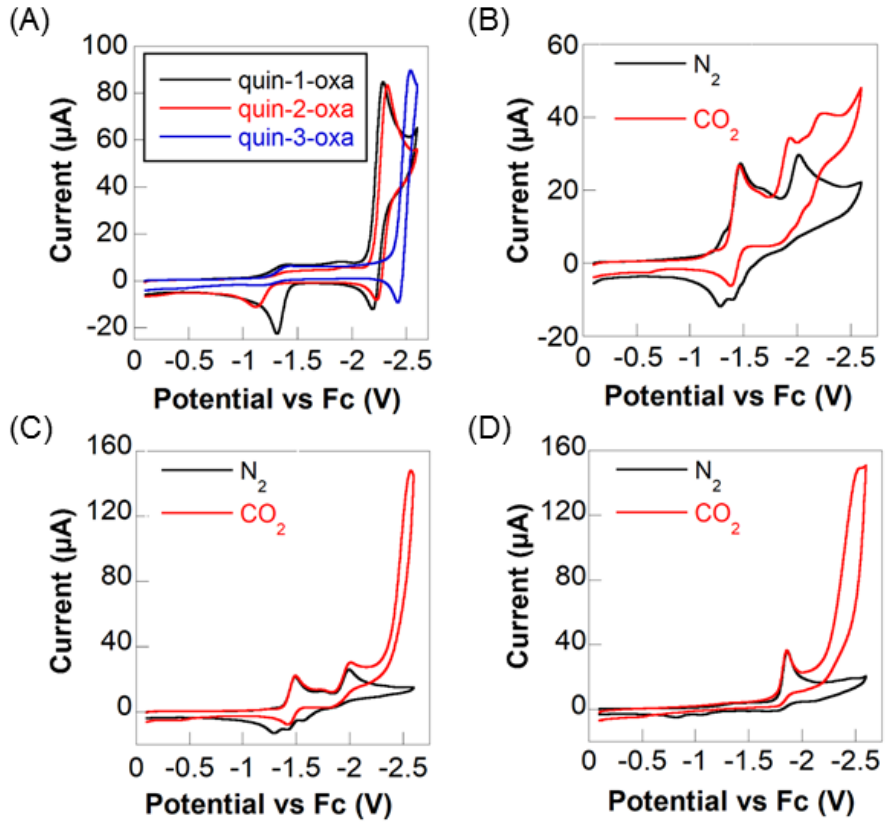

Figure 4. Representative cyclic voltammograms of (A) ligands **quin-1-oxa** (black), **quin-2-oxa** (red), and **quin-3-oxa** (blue), (B) **1**, (C) **2**, and (D) **3** in acetonitrile at a scan rate of 0.1 V/s under N_2 and CO_2. Conditions: 3 mm diameter glassy carbon working electrode, platinum wire counter electrode, 100 mV/s, 1 mM catalyst, 0.1 M $[^nBu_4N]PF_6$, room temperature.

additional feature at ~–1.6 V vs $Fc^{+/0}$ related to the oxidation of $[Re(quin\text{-}2\text{-}oxa)(CO)_3]^-$, as it is not present when the switching potential is set before the second reduction (Figure S11-S12). Between the first and second cathodic peaks, **1** and **2**, one can occasionally observe a shoulder (Figures 4B, 4C, and S16). We propose that the shoulder appears when traces of H_2O is introduced in the system during sparging with the gases. We base our hypothesis in the resemblance of the shoulder with the peaks that appear at ~–1.7 V when H_2O is added (Figure S22). This cathodic peak likely corresponds to the reduction of a rhenium hydride species formed after chloride is displaced from the first coordination sphere. Concentration-dependent

data (Figure S13) and cyclic voltammograms in DMSO and DMF (Figure S18) show that dimeric species, $[Re(quin\text{-}1\text{-}oxa)(CO)_3]_2^-$, of **1** is produced and is oxidized at –0.7 V vs $Fc^{+/0}$ in acetonitrile, and ~–0.5 V in DMSO and DMF.

The first reduction of **3** occurs at a more negative potential, –1.86 V, as compared to **1** and **2**. Unlike the first reduction wave for its congeners **1** and **2**, the first reduction of **3** in the presence of $[^nBu_4N]PF_6$ is irreversible. The one-electron reduced species $[Re(quin\text{-}3\text{-}oxa)(CO)_3Cl]^-$ undergoes equilibrium with $[Re(quin\text{-}3\text{-}oxa)(CO)_3]^0$ after losing a Cl^-. The former species is reduced at –2.5 V, whereas $[Re(quin\text{-}3\text{-}oxa)(CO)_3]^0$ forms a dimer, $[Re(quin\text{-}3\text{-}oxa)(CO)_3]_2$, that is reduced at –2.3 V. When $[^nBu_4N]Cl$ is used as an electrolyte (Figure S12), the Cl^- does not leave the coordination sphere of $[Re(quin\text{-}3\text{-}oxa)(CO)_3Cl]^-$ and the cathodic peak at -2.3 V is no longer present.

Table 1. First reduction peak potentials in the absence of a substrate (E_p),[a] current densities (j),[b] and overpotentials for **1**-**3** in acetonitrile.

Catalyst	*1st reduction potential* (V vs $Fc^{+/0}$)	*2nd reduction potential* (V vs $Fc^{+/0}$)	j (mA/cm^2)	η_{CO} (V)	η_{CH4} (V)
1	-1.47	-2.02	0.57	2.08	2.37
2	-1.49	-2.00	1.26	2.36	2.58
3	-1.86	-2.44	1.22	2.21	2.48
I	-1.75	-2.31	1.31	2.11	
$Re(bpy)(CO)_3Cl$	-1.73	-2.11	0.5		

[a]Cyclic voltammograms were recorded in acetonitrile solution (1.0 mM in catalyst) with 0.1 M $TPAPF_6$ supporting electrolyte, using a 3 mm glassy carbon working electrode, Pt wire counter electrode, Ag/Ag^+ reference electrode (10 mM $AgNO_3$ in acetonitrile), and scan rate 0.1 V/s. [b]Current densities, j, were determined at the potential of $E_{cat/2}$.Overpotential (η) was determined in the absence of a proton donor and from a difference of $E_{cat/2}$ and the CO_2/CO and CO_2/CH_4 couples of −0.12 and +0.15 V vs $Fc^{+/0}$ respectively.[55-56]

Next, we examined the voltammetric response for **1**-**3** under CO_2 saturation. Reductive scans show that little or no catalytic enhancement occurs at the first reduction potential at a scan rate of

0.1 V/s. For complexes **1** and **2**, a shift and a negligible increase in current is observed at the second reduction potential. The onset of more pronounced catalytic currents occurs at –2.15 V and –2.30 V vs $Fc^{+/0}$ for **1** and **2**, respectively. For **3**, the current increases at potentials near the $[Re(quin\text{-}3\text{-}oxa)(CO)_3]^0$/ $[Re(quin\text{-}3\text{-}oxa)(CO)_3]^-$ reduction and peaks at *c.a.* –2.55 V vs $Fc^{+/0}$. The absence of S-shaped plots (Figure 4) reveals that CO_2 reduction by **1-3** is not under kinetic control. Typically, the "foot-of-the-wave analysis" (FOWA) method could allow the extraction of the kinetics parameters; however, in our case the lack of a singular dominant product means that any attempted extraction of k_{cat} will provide unreliable data. Kubiak and co-workers recently reported that in a family of closely related rhenium tricarbonyl complexes, FOWA provided inconsistent k_{cat} values and in disagreement to values obtained by stopped-flow UV-vis spectroscopy.[8] As such, quantification of the catalytic activity of **1-3** will only be limited to relative turnover frequencies ($(i_{cat}/i_p)^2$,TOFs), faradaic efficiencies (FEs) and turnover number (TON) values obtained from controlled potential electrolysis (CPE) studies. First order kinetics with respect to **1** was observed when the concentration of the catalyst was varied from 1 mM to 3 mM (Figures S13 and S14) indicating that catalysis occurs on one rhenium center at these concentrations. The activity of **1**, **2** and **3**, as determined by the increase in the $(i_{cat}/i_p)^2$ value, is negatively affected when DMF and DMSO are used as solvents (Figures S18-S20). We previously reported a similar solvent dependence for a family of rhenium(I) complexes containing pyridine-oxazoline ligands.

To further characterize the electrocatalytic CO_2 conversion, we next examined the voltammetric response for **1-3** in the presence of the Brønsted acids water, methanol, and 2,2,2-trifluoroethanol (TFE) (Figure S21 – S23). Under an atmosphere of N_2 and under increasing protic concentrations, new cathodic peaks are observed. Complexes **1** and **2** present a new peak

at ~–1.7 V in the presence of the three proton donors. When TFE is added, a second new peak is observed at –2.2 V in these two complexes. This peak is not observed when methanol is the proton donor and is only observed for **1** when H_2O is added. Complex **3** shows a broad pre-wave at –1.1 V when the three Brønsted acids are added as well as a shoulder at –2.0 V when TFE is used. For the three complexes, the increase in current at potentials more negative than at –2.0 V indicate that they can catalyze proton reduction, albeit with low activity. The most active proton reduction complex is **1** in the presence of TFE. Under an atmosphere of CO_2, the addition of Brønsted acids leads to a complex behavior (Figures S21-S23). For example, when TFE is used (Figure S21), an increase in current is observed at ~E_{cat} (-2.20 V, -2.36 V, and -2.33 V for **1**, **2**, and **3**, respectively), whereas at the potential at which CO_2 reduction occurs, *c.a.* -2.5 V, a decrease in current at the CO_2 reduction potentials is observed for compounds **2** and **3** upon addition of TFE, while **1** shows an increase in current although not as high as when CO_2 is not present. We propose that this behavior indicates that these complexes have a preference for CO_2 reduction of H^+ reduction.

Preparative-scale electrolysis experiments were carried out with catalysts **1**-**3** to characterize the CO_2 reduction products (Tables 2-4). The experiments were performed for 2 h at two different potentials, E_{cat} and -2.5 V. The liquid and gas phases were analysed by ^{1}H-NMR and GC-MS, respectively. At the more positive potential values, low amounts of CO are formed. The addition of TFE results in the increase of CO formation, five times for **1**, and roughly double for **2** and **3** relative to anhydrous conditions. Remarkably, CH_4 is also observed in the gas chromatograms, although with TON < 1. When the preparative-scale electrolysis experiments were performed at –2.5 V (vs $Fc^{+/0}$) CH_4 was detected. In isotope labelling experiments conducted under a $^{13}CO_2$ atmosphere, GC-MS analysis identified as reaction product $^{13}CH_4$ (m/z

= 17), confirming that methane originates from CO_2 reduction (Figure S29 - S31). The production of CH_4 also increased when the potential was –2.5 V, reaching TON that ranged from 1.5 ± 0.1 to 1.7 ± 0.1 after 2 hours of electrolysis. Addition of Brønsted acids when the bulk electrolysis was performed at -2.5 V increased the production of CH_4. TFE was the best additive for the production of CH_4, making the reaction catalytic (TON = 1.8, 1.6, and 1.3 for **1**, **2**, and **3**, respectively). No liquid products were detected in any of the aforementioned conditions. Evolution of methane also occurs from preparative-scale electrolysis of $[Re(quin\text{-}n\text{-}oxa)(CO)_4]^+$ under a CO-saturated acetonitrile solution, suggesting that CO is an intermediate in the formation of methane (Figure S37). Additional CPE experiments with increasing concentrations of catalysts, from 1 mM to 3 mM in CH_3CN, show increase formation of CO and methane (Table S2).

During the catalytic formation of methane from CO_2, one can expect that hydroxycarbene and hydroxymethyl species form as intermediates (*vide infra*). Thus, we performed preparative-scale electrolysis experiments under N_2 but in the presence of formaldehyde and methanol (Figures S39 and S40). In both cases, we observed small amounts of methane, although the amounts are negligible when compared to reactions in the presence of CO_2 they provide additional evidence for the posible formation of the aforementioned intermediates. The small amount of methane produced is probably due to the fact that rhenium-hydroxycarbene and -hydroxymethyl species are not favored under these reaction conditions.

Table 2. Faradaic efficiencies, turnover numbers (TON) and turnover frequencies (TOF) for **1** in acetonitrile after CPE experiments (triplicate runs) with a reticulated vitreous carbon working electrode held at different potentials for 2 hours. TOF obtained from CPE. Proton donors were used as indicated at 0.13 M, 0.25 M, and 0.55 M for TFE, MeOH, and H_2O, respectively.

Applied potential (V vs $Fc^{+/0}$)	**Proton donor**	**Faradaic efficiency (%)**			**TON**			**TOF (h^{-1})**		
		H_2	CO	CH_4	H_2	CO	CH_4	H_2	CO	CH_4
-2.2 ($E_{cat/2}$)	-	<1	8 ± 1%	-	<1	0.6	-	-	0.3	-
-2.2 ($E_{cat/2}$)	TFE	<1	43 ± 4%	19 ± 3%	<1	2.5	0.8	-	1.25	0.4
-2.5	-	<1	35 ± 2%	25 ± 3%	<1	1.5	1.1	-	0.75	0.55
-2.5	TFE	<1	45 ± 4%	31 ± 3%	<1	2.4	1.8	-	1.2	0.9
-2.5	MeOH	<1	38 ± 2%	21 ± 3%	<1	1.7	0.9	-	0.85	0.45
-2.5	H_2O	<1	39 ± 2%	19 ± 3%	<1	1.7	0.9	-	0.85	0.45

Table 3. Faradaic efficiencies, turnover numbers (TON) and turnover frequencies (TOF) for **2** in acetonitrile after CPE experiments (triplicate runs) with a reticulated vitreous carbon working electrode held at different potentials for 2 hours. TOF obtained from CPE. Proton donors were used as indicated at 0.13 M, 0.25 M, and 0.55 M for TFE, MeOH, and H_2O, respectively.

Applied potential (V vs $Fc^{+/0}$)	**Proton donor**	**Faradaic efficiency (%)**			**TON**			**TOF (h^{-1})**		
		H_2	CO	CH_4	H_2	CO	CH_4	H_2	CO	CH_4
-2.4 ($E_{cat/2}$)	-	<1	8 ± 2%	-	<1	0.8	-	-	0.4	-
-2.4 ($E_{cat/2}$)	TFE	<1	16 ± 4%	8 ± 1%	<1	0.9	0.4	-	0.45	0.2
-2.5	-	<1	31 ± 3%	28 ± 3%	<1	1.7	1.1	-	0.85	0.55
-2.5	TFE	<1	39 ± 3%	34 ± 1%	<1	2.6	1.6	-	1.3	0.8
-2.5	MeOH	<1	24 ± 2%	29 ± 2%	<1	1.4	1.1	-	0.7	0.55
-2.5	H_2O	<1	26 ± 3%	31 ± 2%	<1	1.4	1.2	-	0.7	0.6

Table 4. Faradaic efficiencies, turnover numbers (TON) and turnover frequencies (TOF) for **3** in acetonitrile after CPE experiments (triplicate runs) with a reticulated vitreous carbon working electrode held at different potentials for 2 hours. TOF obtained from CPE. Proton donors were used as indicated at 0.13 M, 0.25 M, and 0.55 M for TFE, MeOH, and H_2O, respectively.

Applied potential (V vs $Fc^{+/0}$)	Proton donor	Faradaic efficiency (%)			TON			TOF (h^{-1})		
		H_2	CO	CH_4	H_2	CO	CH_4	H_2	CO	CH_4
-2.3 ($E_{cat/2}$)	-	<1	11 ± 1%	-	<1	0.7	-	-	0.35	-
-2.3 ($E_{cat/2}$)	TFE	<1	28 ± 3%	30 ± 3%	<1	1.4	1	-	0.7	0.5
-2.5	-	<1	35 ± 4%	29 ± 2%	<1	1.7	1	-	0.7	0.5
-2.5	TFE	<1	39 ± 2%	33 ± 3%	<1	1.9	1.3	-	0.95	0.65
-2.5	MeOH	<1	30 ± 3%	23 ± 1%	<1	1.6	0.9	-	0.8	0.45
-2.5	H_2O	<1	33 ± 2%	25 ± 3%	<1	1.7	1	-	0.85	0.5

Infrared-Spectroelectrochemistry

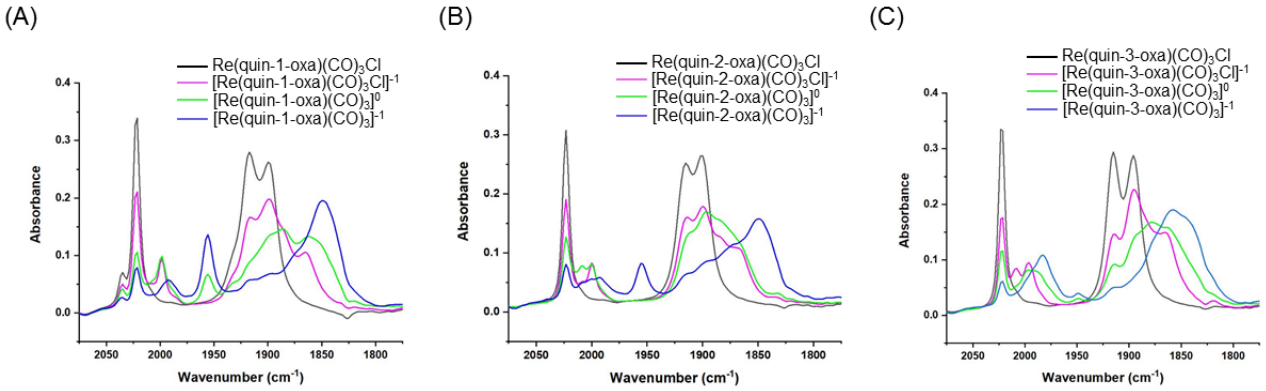

Figure 5. Infrared-Spectroelectrochemistry spectra of the reduction of **1** (left), **2** (center), and **3** (right) in acetonitrile under Ar with 0.1 M $TBAPF_6$ as a supporting electrolyte.

We examined the species formed upon reduction of complexes **1**, **2** and **3** using IR-SEC (Figure 5 and Table 5), a technique that has previously been used for elucidating the behavior of Re and Mn-based CO_2 reduction catalysts, including the parent complex **I**.[18, 57-64] At resting

potential, complexes **1**-**3** are the only species observed in solution. As more negative potentials are applied, the signals for the starting materials disappear, with the simultaneous appearance of new bands at lower frequencies (~13-34 cm^{-1}). This is consistent with a ligand-based reduction of the parent complexes. However, these species are relatively short-lived, and allowing this species to stand in solution without changing the potential results in new species with signals that are an additional 6-21 cm^{-1} more negative. We attribute this to the loss of Cl^- and the charge transfer from the *quin-n-oxa* ligands to the Re metal, analogous to the parent complex **I**.[36] The species observed in this state were difficult to obtain as clean spectra because they often coexisted with the Cl^- bound species and the further reduced anion. As the cell potential is swept further negative, the $[Re(quin\text{-}n\text{-}oxa)(CO)_3]^0$ species corresponding to **1** and **2** are reduced to the anion $[Re(pyroxa)(CO)_3]^-$. The overall shift from **1** and **2** to their doubly reduced species (~65 cm^{-1}) is reminiscent of those found for other rhenium complexes and assigned to a final Re^0 redox state with the additional electron on the bidentate azine ligand.[64] For **3**, holding the potential at the first reduction for a longer time results in new ν_{CO} modes observed at 1982, 1945, 1863, and 1842 cm^{-1}. These frequencies probably correspond to the formation of the dimeric species $[Re(quin\text{-}3\text{-}oxa)(CO)_3]_2$. Such dimerization is well known for $Re(bpy)(CO)_3Cl$ and related species if the bidentate ligand is not too sterically bulky.[23] We also examined compound **2** with tetrabutylammonium chloride as the supporting electrolyte (Figure S42), and only observed the mono-reduced $[Re(quin\text{-}2\text{-}oxa)(CO)_3Cl]^-$ species, and the doubly-reduced $[Re(quin\text{-}2\text{-}oxa)(CO)_3]^-$ anion, consistent with the cyclic voltammetry shown in Figure S12, indicating that the excess chloride prevents Cl^- dissociation from the initially mono- reduced species until it is reduced a second time.

Table 5. Signals observed in IR-SEC spectra of compound **1-3** in acetonitrile under Ar with 0.1 M $TBAPF_6$ as a supporting electrolyte.

Species	n = 1	n = 2	n =3
Re((quin-n-oxa)$(CO)_3$Cl	2022, 1917, 1899	2023, 1915, 1900	2023, 1915, 1896
[Re((quin-n-oxa)$(CO)_3$Cl]$^{-1}$	1998, 1885, 1865	1999, 1886, 1866	1997, 1884, 1865
[Re(quin-n-oxa)$(CO)_3$]^{0}	1956, 1886, 1863	2008, 1897, 1864	1990, 1878, 1864
[Re(quin-n-oxa)$(CO)_3$]$^{-1}$	1956, 1849	1955, 1849	1948, 1856

Theoretical Investigation of the CO_2 Reduction Mechanism

The electrocatalytic reduction of CO_2 to CO and CH_4 was studied using density functional theory at the M06 level of theory with SMD continuum solvation for acetonitrile and the proposed mechanisms are summarized in Schemes 1-4.

CO Evolution Mechanism

The proposed reaction mechanism for CO evolution for complexes **1-3** is presented in Scheme 1 along with the computed reduction potentials, pK_as, free energy changes (ΔG) and activation free energies ($\Delta G^{‡}$). One electron reduction potentials of ligands **quin-1-oxa**, **quin-2-oxa** and **quin-3-oxa** are computed to be –2.13 V, –2.16 V and –2.39 V vs $Fc^{+/0}$ in quite good agreement with experimental observations, especially in terms of the cathodic shift in the reduction potential of **quin-3-oxa** ligand. A similar trend is observed for the one electron reduction of **[Re–Cl]** to **[Re–Cl]**$^{–}$ with computed reduction potentials of –1.43 V, –1.50 V and –1.91 V vs $Fc^{+/0}$ respectively for complexes **1**, **2** and **3**. The spin population data of **[Re–Cl]**$^{–}$ complexes (and **[Re]^{0}** formed upon chloride dissociation) indicates that the additional $e^{–}$ is mostly localized on the ligand (Figure S40-42). The second reduction step could proceed via

different pathways starting from **[Re–Cl]**$^{-}$ (Scheme 1) and among the pathways examined the reduction of **[Re–Cl]**$^{-}$ to **[Re]**$^{-}$ and chloride anion (–1.81 V, –1.83 V and –2.18 V vs $Fc^{+/0}$ respectively for complexes **1**, **2** and **3)** provided the best agreement with experimentally observed potentials whereas the reduction of **[Re]**^{0} to **[Re]**$^{-}$ yielded more positive computed potentials (–1.58 V, –1.59 V and –1.98 V vs $Fc^{+/0}$ respectively for complexes **1**, **2** and **3)**. The following CO_2 binding to doubly reduced **[Re]**$^{-}$ to generate **[Re–CO_2]**$^{-}$ is surprisingly quite unfavorable for **1** and **2** (ΔG of about 20 kcal/mol) whereas it's uphill by only 5 kcal/mol for **3** in line with the electrochemical data displaying significant differences in the enhancement of second reduction peaks of **1** and **2** versus **3** in the presence of CO_2. In contrast, CO_2 binding to **[Re]**$^{2-}$ to form **[Re–CO_2]**$^{2-}$ is favorable for all three complexes (ΔG of –2.8 to –5.5 kcal/mol). However, further reduction of **[Re]**$^{-}$ to **[Re]**$^{2-}$ requires highly negative applied potentials (–2.93 V, –2.92 V and –2.65 V vs $Fc^{+/0}$ respectively for complexes **1**, **2** and **3,** Table 3**)** and not likely to occur especially for **1** and **2**. The protonation of **[Re–CO_2]**$^{-}$ will yield **[Re–CO_2H]**^{0} for which computed pK_as are 24.3, 25.5 and 28.4, respectively for complexes **1**, **2** and **3,** so that in the presence of a favorable Brønsted acid and fast protonation kinetics, CO_2 binding to **[Re]**$^{-}$ might proceed for complexes **1** and **2** as well. This is reminiscent of the behavior of tricarbonyl Mn-Bpy type complexes where CO_2 binding after formation of $2e^{-}$ reduced species requires the presence of Brønsted acids.[28] This is further supported by the changes in CVs in the presence of CO_2 and 2,2,2-trifluoroethanol (TFE) as a Brønsted acid for complexes **1-3**. Upon formation of **[Re–CO_2H]**^{0}, generation of CO could proceed via either *protonation first* or *reduction first* pathway, and we explored both pathways using water, methanol and TFE as the Brønsted acids. Here, only the data for TFE will be presented and similar data for water and methanol is available in the supporting information (Table S4 and Figures S46-48). The *protonation first*

pathway starts with C–OH bond cleavage of **[Re–CO$_2$H]^0** intermediate assisted by TFE with a computed activation free energy ($\Delta G^{\ddagger}$) of 21.1, 22.2 and 25.5 kcal/mol for complexes **1-3** respectively, generating **[Re–CO]$^+$**, which upon reduction forms **[Re–CO]^0**. In contrast, the *reduction first* pathway starts with reduction of **[Re–CO$_2$H]^0** to **[Re–CO$_2$H]$^-$** followed by C–OH bond cleavage, which features $\Delta G^{\ddagger}$ of 18.9, 18.2 and 22.4 kcal/mol for complexes **1-3** respectively, generating the common **[Re–CO]^0** product. Further reduction of **[Re–CO]^0** could result in evolution of CO and regeneration of active **[Re]$^-$** intermediate. We note that although the proposed CO evolution mechanism is similar to that of Re(bpy)(CO)$_3$Cl, **1-2** exhibit distinct behavior such as diminished reactivity towards CO_2 from doubly reduced **[Re]$^-$** species and stronger affinity towards CO product as well as complex behavior in the presence of Brønsted acids which could stem from possible protonation of the ligands. The latter is expected to play a significant role in CH_4 generation as discussed next.

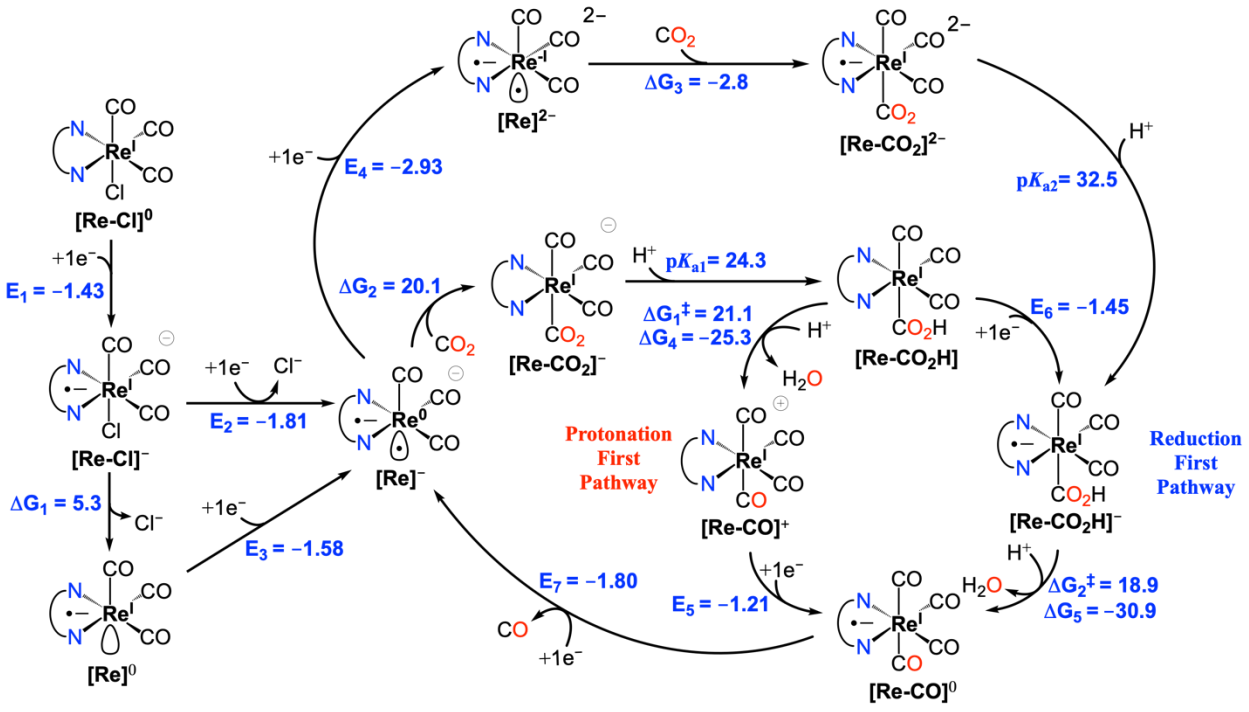

	1	2	3

$\mathbf{E_1}$	–1.43	–1.50	–1.91
$\mathbf{E_2}$	–1.81	–1.83	–2.18
$\mathbf{\Delta G_1}$	5.3	5.6	4.7
$\mathbf{E_3}$	–1.58	–1.59	–1.98
$\mathbf{\Delta G_2}$	20.1	19.4	5.0
$\mathbf{p}K_{\mathbf{a1}}$	24.3	25.5	28.4
$\mathbf{E_4}$	–2.93	–2.92	–2.65
$\mathbf{\Delta G_3}$	–2.8	–3.8	–5.5
$\mathbf{p}K_{\mathbf{a2}}$	32.5	31.1	32.7
$\mathbf{\Delta G_1}^{\ddagger}$	21.1	22.2	25.5
$\mathbf{\Delta G_4}$	–25.3	–24.9	–24.7
$\mathbf{E_5}$	–1.21	–0.91	–1.71
$\mathbf{E_6}$	–1.45	–1.58	–1.94
$\mathbf{\Delta G_2}^{\ddagger}$	18.9	18.2	22.4
$\mathbf{\Delta G_5}$	–30.9	–31.6	–29.9
$\mathbf{E_7}$	–1.80	–1.88	–2.24

Scheme 1. Proposed reaction mechanism for electrocatalytic CO_2 reduction to CO by complexes **1-3** (top) and associated energetics of designated steps (bottom). The energetics associated with complex **1** are also shown in the proposed mechanism. The computed reduction potentials (E) are in units of volts versus $Fc^{+/0}$, and the free energy changes (ΔG) and activation free energies ($\Delta G^{\ddagger}$) are in units of kcal/mol at pH 0. The computed pK_as are for the corresponding conjugate acids in the protonation steps. The C-OH bond cleavage steps ($\Delta G_1^{\ddagger}$, $\Delta G_2^{\ddagger}$) involve TFE as the proton donor.

CH_4 Generation Mechanism

Next, we turned our attention to possible reaction routes for CH_4 formation and hypothesized two possible pathways based on generation of hydride donors to further reduce CO to CH_4 which are presented in Schemes 2-4 for complex **1**. The first pathway involves protonation of the metal center (pK_a = 18.0) in $[Re(quin\text{-}1\text{-}oxa)(CO)_3]^-$ to generate a rhenium hydride, [**Re-quin-1-oxa-H**]$^{\mathbf{0}}$ (Scheme 2), with a computed hydricity of 36.9 kcal/mol (2.1 kcal/mol stronger hydride donor than $[Ru(tpy)(bpy)H]^+$, ΔG_{H^-} = 39 kcal/mol).[65-67] We explored possible hydride and

hydrogen atom transfer reactions between several **[Re-quin-1-oxa-H]^{m}** and **[Re-quin-1-oxa-CO]^{n}** couples (Figure S49-53) and found the reaction of [**Re-quin-1-oxa-H**] with **[Re-quin-1-oxa-CO]$^{+}$** to afford the formyl species (ΔG = 4.2 kcal/mol) to be more favorable than other alternatives investigated. Sequential hydride transfer from [**Re-quin-1-oxa-H**] to formyl species and protonation steps will eventually generate CH_4 (Figure S49-53). However, we note that the initial formation of [**Re-quin-1-oxa-H**]^{0} is predicted to be kinetically hindered ($\Delta G_2^{\ddagger}$ = 42.3 kcal/mol, Scheme 2) and even if it is formed the more likely CO_2 reduction product will be formate rather than CH_4 in the presence of rhenium hydride species.

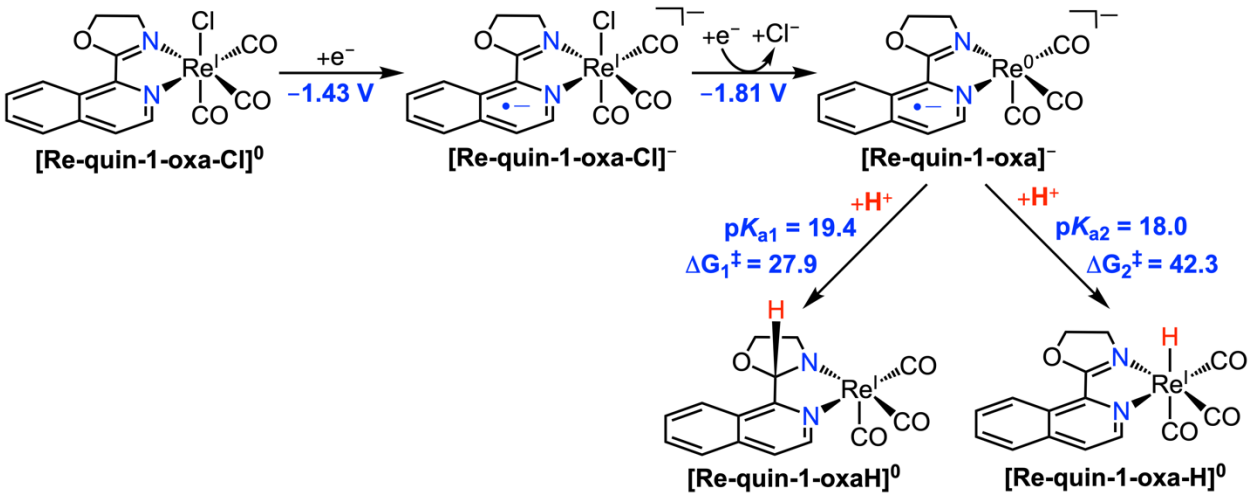

Scheme 2. Proposed mechanism of hydride intermediate generation for complex **1**. The computed reduction potentials (E) are in units of volts versus $Fc^{+/0}$ and the computed pK_as are for the corresponding conjugate acids in the protonation steps. The protonation steps ($\Delta G_1^{\ddagger}$, $\Delta G_2^{\ddagger}$) involve TFE as the proton donor.

On the other hand, the protonation of the carbon atom of the C=N group on the oxazoline ring (pK_a = 19.4) in $[Re(quin\text{-}1\text{-}oxa)(CO)_3]^{-}$ is also possible (Scheme 2) and kinetically more favorable by 14.4 kcal/mol compared to generation of [**Re-quin-1-oxa-H**]^{0}, which led us to the

second proposed pathway as summarized Schemes 3-4. [**Re-quin-1-oxa-CO**]^{0} (*reduction first pathway* product as stated above) can be reduced to [**Re-quin-1-oxa-CO**]$^{-}$ and, rather than evolving CO, could get protonated at the ligand (pK_a 21.6) to produce a [**Re(quin-1-oxaH)-CO**] species that can react intramolecularly to produce **[Re-quin-1-oxa-CHO]** via relatively low activation free energy ($\Delta G^{\ddagger}$ = 18.9 kcal/mol, ΔG = 1.3 kcal/mol) (Scheme 3, Figure S54). Ligand protonation has been previously reported in rhenium-based CO_2 reduction catalysts, although the complex is not directly related to the current family of complexes.[14] Sequential hydride transfer steps together with protonation steps could lead to formation of hydroxycarbene, hydroxymethyl and methane from formyl species and one plausible pathway is depicted in Scheme 4. The unique properties of efficient storage of reducing equivalents (especially for complex **1** and **2**) and ability to generate ligand-based hydride species are thought to be critical for CH_4 generation by complexes **1-3**.

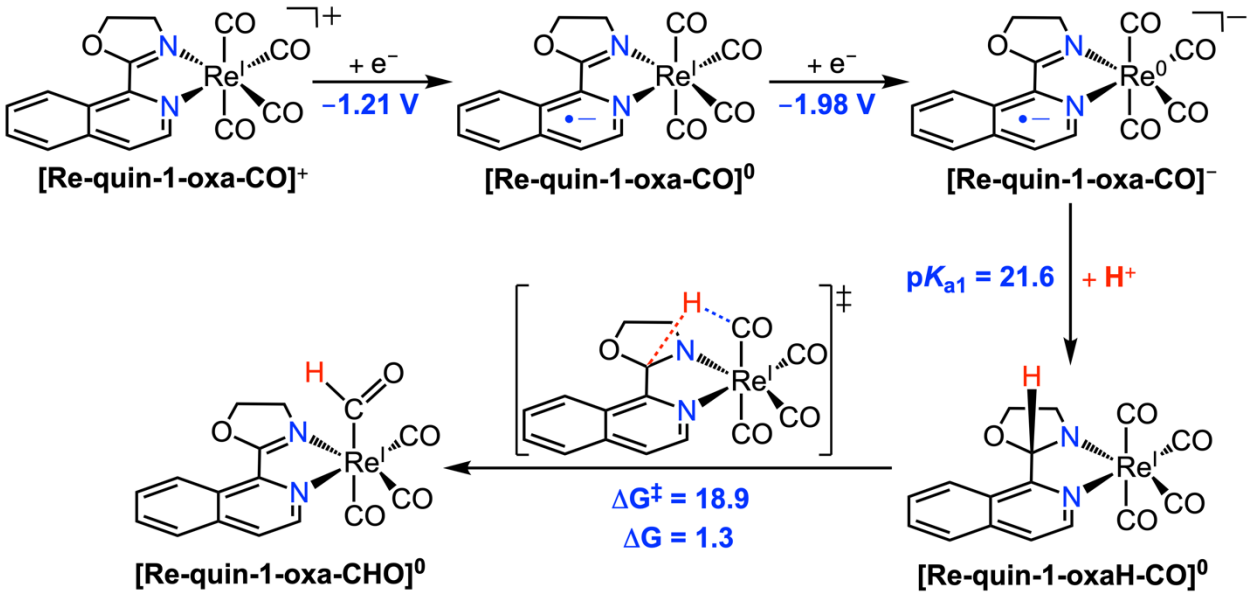

Scheme 3. Proposed reaction mechanism for **quin-1-oxa** ligand-based hydride formation and hydride transfer to generate formyl anion intermediate. The computed reduction potentials (E) are in units of volts versus $Fc^{+/0}$, and the free energy changes (ΔG) and activation free energies

($\Delta G^{\ddagger}$) are in units of kcal/mol at pH 0. The computed pK_as are for the corresponding conjugate acids in the protonation steps.

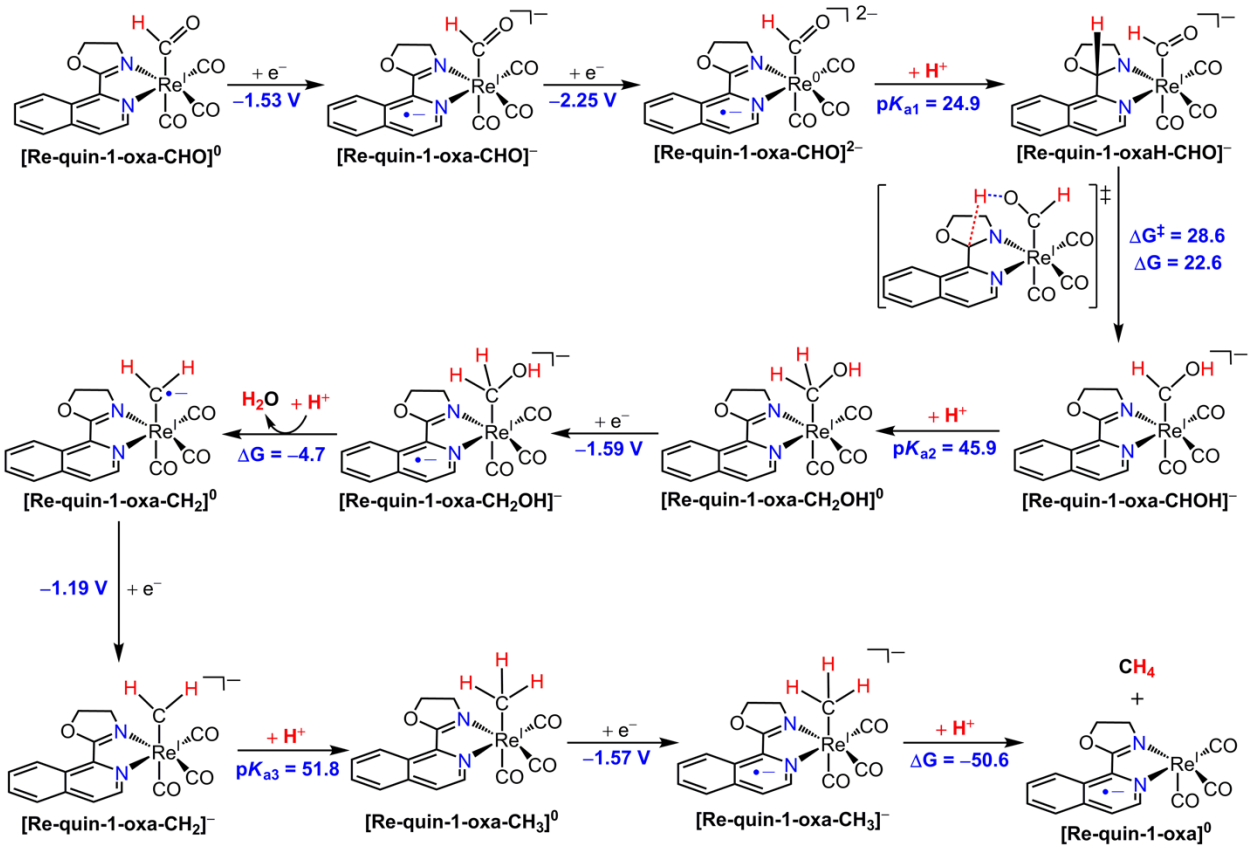

Scheme 4. Proposed reaction mechanism for methane generation starting from formyl anion intermediate. The computed reduction potentials (E) are in units of volts versus $Fc^{+/0}$, free energy changes (ΔG) and activation free energies ($\Delta G^{\ddagger}$) are in units of kcal/mol at pH 0. The computed pK_as are for the corresponding conjugate acids in the protonation steps.

It should be noted that given the reactivity of the ligands and low stability of the complexes **1-3** in CO_2 reduction conditions, the transformation of catalysts to other reactive intermediates could not be ruled out. One such example is attack of basic molecules such as

hydroxide, which could form during water assisted C-OH bond cleavage step, to the carbon atom of the C=N group on the oxazoline ring to transform the ligand and the complex (Figure S55).

Discussion

Catalysts **1-3** are the first examples of rhenium complexes capable of catalysing the conversion of CO_2 to CH_4. Compounds **1** and **2** are inactive in their doubly reduced state since CO_2 binding is endergonic. Kubiak et al. has recently shown for two $Re(bpy\text{-}R)(CO)_3Cl$ complexes with electron withdrawing substituents (R = CN or CF_3) that they require a third reduction for CO_2 catalysis. The additional electron density enhances the nucleophilicity of the $[Re(bpy\text{-}R)(CO)_3]^{2-}$ complex, but in exchange they undergo degradation fairly easily as a result of destabilization of the molecular framework.[8] The latter is the likely cause of the observed low FE values by the complexes in the current study. While the presence of the extended π-system leads to a destabilizing third reduction event it also confers the ability for **1** and **2** to evolve methane by enabling an equilibrium shift, away from CO dissociation. This means in the final reductive step of the tetracarbonyl intermediate in the catalytic cycle to release CO, a significant portion of the CO remains bound, which enables further reactivity to methane. Maintaining a stable tetracarbonyl intermediate under catalytically reducing conditions is inherently difficult. This difficulty was recognized in an earlier study by Tanaka and coworkers who sought to achieve the multielectron reduction of CO_2 by the $[Ru(bpy)_2(CO)_2]^{2+}$ complex but were unsuccessful.[68] However, upon switching to the $[Ru(bpy)(tpy)(CO)]^{2+}$, complex they were able to catalytically afford a relatively stable carbonyl intermediate and thus observe several multielectron reduction products such as CH_3OH.[69] In principle, homogeneous systems for the activation of CO_2 to CH_4 were unknown until recently when reports by Robert et al.,[70-71] and Jurss et al.,[72] elegantly affirmed the possibility of the multielectron reduction of CO_2 to CH_4 by

homogeneous metal complexes. Though the reports are scarce in mechanistic details, Robert et al. in their work attest to the presence of an Fe^{II}-CO intermediate that is stable enough for eventual reduction to CH_4.[71] The dissociation of CO to afford the catalytic resting states $[Re(bpy)(CO)_3]^-$ and $[Re(pyroxa)(CO)_3]^-$ occurs spontaneously when $[Re(bpy)(CO)_4]^0$ and $[Re(pyroxa)(CO)_4]^0$ is further reduced.[36, 73] On the other hand, $[Re(quin\text{-}1\text{-}oxa)(CO)_4]^-$ is a stable intermediate, and CO dissociation proceeds with a computed ΔG of –4.3 kcal/mol. This reveals that the delocalization of the electron density on the ligand scaffold upon reduction confers a stable tetracarbonyl intermediate for **1** and by extension for **2**, which enhances further reactivity of this reactive axial carbonyl ligand. We also note that for the Mn analog, we could not locate a stable optimized structure for $[Mn(quin\text{-}1\text{-}oxa)(CO)_4]^-$ intermediate, and observed spontaneous CO evolution upon reduction of $[Mn(quin\text{-}1\text{-}oxa)(CO)_4]^0$, which could explain the observation of CO as the sole product for the recently reported tricarbonyl Mn complex of quinoxa ligand.[3]

As mentioned above, we hypothesize that the presence of protic sources facilitates ligand protonation to afford methane evolution (and probably a competing parallel mechanism that leads to ligand degradation). To justify that ligand protonation is a key mechanistic step for the evolution of methane, we synthesized the *fac*-Re(2-(pyridin-2-yl)quinoline)$(CO)_3Cl$ complex (**4**) where its ligand framework consists of a pyridyl group in the place of the oxazoline moiety. The electrochemical behavior was then probed via cyclic voltammetry while product distribution and selectivity were analyzed via CPE. Preparation of *fac*-Re(2-(pyridin-2-yl)quinoline)$(CO)_3Cl$ (**4**) was carried out in analogy with the method utilized for **1**-**3** (see SI).

The electrochemical behavior of the **4** closely resembles the redox behavior of **1** and **2**. The first reversible reduction couple is ligand based with a cathodic peak potential E_p at –1.55 V vs $Fc^{+/0}$ and a return anodic wave at E_p = –1.49 V vs $Fc^{+/0}$. The second reduction step occurs at E_p =

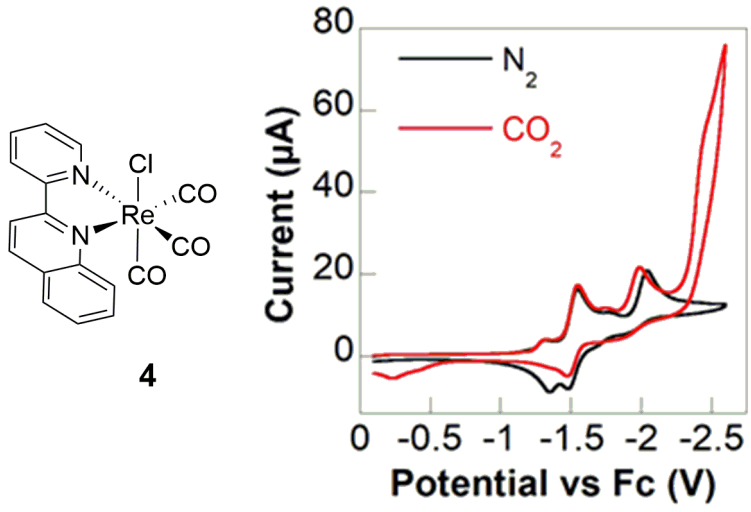

Figure 6. Structural representation of the rhenium complex **4** and the representative cyclic voltammogram of **4** in acetonitrile at a scan rate of 0.1 V/s under N_2 and CO_2. Conditions: 3 mm diameter glassy carbon working electrode, platinum wire counter electrode, 1 mM catalyst, 0.1 M $TBAPF_6$, room temperature.

–2.05 V vs $Fc^{+/0}$. Catalytic behavior of **4**, mirrors that observed for compound **1** and **2** in that the onset of the catalytic wave occurs at a potential more negative than the second reduction step. Preparative scale electrolysis of **4** reveal the FE for CO evolution is 25 ± 2%, and it compares in a similar manner to the measured values for the complexes **1**-**3** (Table 2-4). This similarity of FE reveals that **4** is also a sluggish catalyst. Only trace amounts of methane are observed during the controlled potential electrolysis of **4** under CO_2 atmosphere (Table S3). This result supports the key role of the oxazoline ligand in the catalytic formation of CH_4, likely as a hydride storage and transfer agent. Furthermore CPE studies as a function of catalyst concentration reveal first order kinetics (Table S2) expected of an intramolecular hydride based mechanism rather than a bimolecular mechanism as proposed by computational calculations. The small amount of methane formed in the presence of **4** also supports the plausibility of a rhenium hydride intermediate as the second, less favorable, alternative pathway for methane formation.

Conclusions

In conclusion, we have prepared the first family of rhenium complexes capable of electrochemically reducing carbon dioxide to methane. Despite the fact that the complexes are not efficient at producing methane, they join a very small group of known molecular catalysts capable of reducing CO_2 to methane. Our combined experimental and theoretical studies predict two possible hydride donors for methane generation from CO, a rhenium-hydride and a protonated oxazoline ligand. The ligand assisted pathway is more efficient at assisting the further reduction of CO, however we also cannot rule out interactions between acidic and basic species in solution with the ligand via pathways that are detrimental to the stability of the complex. The results also highlight the key role of ligand-based reduction processes in the vicinity of the metal center in enabling CO_2 reduction past the 2-electron product CO. Delocalization of the electron density on the ligand scaffold upon reduction stabilizes the key carbonyl intermediate leading to additional reactivity of this ligand. This insight should aid the development of more efficient catalytic systems to reduce CO_2 into CH_4 and other C_n products under mild conditions.

Conflicts of interest

There are no conflicts to declare.

Acknowledgments

A.M.A.-B. is grateful for support from the National Science Foundation CAREER grant (CHE-1652606). The work at BNL (M.Z.E) was carried out with support from the U.S. Department of Energy, Office of Science, Division of Chemical Sciences, Geosciences & Biosciences, Office of Basic Energy Sciences under contract DE-SC0012704. C.S. acknowledges the Illinois Louis

Stokes Alliance for Minority Participation (ILSAMP) program for support (National Science Foundation Grant 1411219) as well as the McNair Scholars Program.

ASSOCIATED CONTENT

Supporting Information

The Supporting Information is available free of charge on the ACS Publications website.

^{1}H NMR, ^{13}C NMR, cyclic voltammograms, and computational data (PDF).

Crystallographic data (CIF).

References

1. Nerem, R. S.; Beckley, B. D.; Fasullo, J. T.; Hamlington, B. D.; Masters, D.; Mitchum, G. T., Climate-change-driven accelerated sea-level rise detected in the altimeter era. *Proc. Nat. Acad. Sci.* **2018,** *115*, 2022-2025.

2. White, T. A.; Maji, S.; Ott, S., Mechanistic insights into electrocatalytic CO_2 reduction within $[Ru^{II}(tpy)(NN)X]^{n+}$ architectures. *Dalton Transactions* **2014,** *43* (40), 15028-15037.

3. Steinlechner, C.; Roesel, A. F.; Oberem, E.; Päpcke, A.; Rockstroh, N.; Gloaguen, F.; Lochbrunner, S.; Ludwig, R.; Spannenberg, A.; Junge, H.; Francke, R.; Beller, M., Selective Earth-Abundant System for CO_2 Reduction: Comparing Photo- and Electrocatalytic Processes. *ACS Catalysis* **2019,** *9* (3), 2091-2100.

4. Ulmer, U.; Dingle, T.; Duchesne, P. N.; Morris, R. H.; Tavasoli, A.; Wood, T.; Ozin, G. A., Fundamentals and applications of photocatalytic CO_2 methanation. *Nature Commun.* **2019,** *10* (1), 3169.

5. Wang, M.; Torbensen, K.; Salvatore, D.; Ren, S.; Joulié, D.; Dumoulin, F.; Mendoza, D.; Lassalle-Kaiser, B.; Işci, U.; Berlinguette, C. P.; Robert, M., CO_2 electrochemical catalytic reduction with a highly active cobalt phthalocyanine. *Nature Commun.* **2019,** *10* (1), 3602-3602.

6. Stanton, C. J., III; Machan, C. W.; Vandezande, J. E.; Jin, T.; Majetich, G. F.; Schaefer, H. F., III; Kubiak, C. P.; Li, G.; Agarwal, J., Re(I) NHC Complexes for Electrocatalytic Conversion of CO_2. *Inorg. Chem.* **2016,** *55* (6), 3136-3144.

7. Talukdar, K.; Sinha Roy, S.; Amatya, E.; Sleeper, E. A.; Le Magueres, P.; Jurss, J. W., Enhanced Electrochemical CO2 Reduction by a Series of Molecular Rhenium Catalysts Decorated with Second-Sphere Hydrogen-bond Donors. *Inorg. Chem.* **2020,** *59*, 6087-6099.

8. Clark, M. L.; Cheung, P. L.; Lessio, M.; Carter, E. A.; Kubiak, C. P., Kinetic and Mechanistic Effects of Bipyridine (bpy) Substituent, Labile Ligand, and Bronsted Acid on Electrocatalytic CO_2 Reduction by Re(bpy) Complexes. *ACS Catalysis* **2018,** *8* (3), 2021-2029.

9. Su, X.; McCardle, K. M.; Chen, L.; Panetier, J. A.; Jurss, J. W. Robust and Selective Cobalt Catalysts Bearing Redox-Active Bipyridyl-NHC Frameworks for Electrochemical CO_2 Reduction in Aqueous Solutions. *ACS Catal.* **2019**, *9*, 7398-7408.

10. Cheung, P. L.; Machan, C. W.; Malkhasian, A. Y. S.; Agarwal, J.; Kubiak, C. P., Photocatalytic Reduction of Carbon Dioxide to CO and HCO_2H Using fac-Mn(CN)(bpy)$(CO)_3$. *Inorganic chemistry* **2016,** *55* (6), 3192-3198.

11. Johnson, B. A.; Agarwala, H.; White, T. A.; Mijangos, E.; Maji, S.; Ott, S., Judicious Ligand Design in Ruthenium Polypyridyl CO_2 Reduction Catalysts to Enhance Reactivity by Steric and Electronic Effects. *Chemistry – A European Journal* **2016,** *22* (42), 14870-14880.

12. Johnson, B. A.; Maji, S.; Agarwala, H.; White, T. A.; Mijangos, E.; Ott, S., Activating a Low Overpotential CO_2 Reduction Mechanism by a Strategic Ligand Modification on a Ruthenium Polypyridyl Catalyst. *Angewandte Chemie International Edition* **2016,** *55* (5), 1825-1829.

13. Dalle, K. E.; Warnan, J.; Leung, J. J.; Reuillard, B.; Karmel, I. S.; Reisner, E., Electro- and Solar-Driven Fuel Synthesis with First Row Transition Metal Complexes. *Chem Rev* **2019,** *119* (4), 2752-2875.

14. Manbeck, G. F.; Muckerman, J. T.; Szalda, D. J., Himeda, Y.; Fujita, E., Push or Pull? Proton Responsive Ligand Effects in Rhenium Tricarbonyl CO2 Reduction Catalysts. *J. Phys. Chem B* **2015,** *119*, 7457-7466.

15. Elgrishi, N.; Chambers, M. B.; Wang, X.; Fontecave, M., Molecular polypyridine-based metal complexes as catalysts for the reduction of CO_2. *Chem Soc Rev* **2017,** *46* (3), 761-796.

16. Neyhouse, B. J.; White, T. A., Modifying the steric and electronic character within Re(I)-phenanthroline complexes for electrocatalytic CO_2 reduction. *Inorg. Chim. Acta* **2018,** *479*, 49-57.

17. Ngo, K. T.; McKinnon, M.; Mahanti, B.; Narayanan, R.; Grills, D. C.; Ertem, M. Z.; Rochford, J., Turning on the Protonation-First Pathway for Electrocatalytic CO_2 Reduction by Manganese Bipyridyl Tricarbonyl Complexes. *J. Am. Chem. Soc.* **2017,** *139* (7), 2604-2618.

18. Cuellar, E.; Pastor, L.; García-Herbosa, G.; Nganga, J.; Angeles-Boza, A. M.; Diez-Varga, A.; Torroba, T.; Martín-Alvarez, J. M.; Miguel, D.; Villafañe, F., (1,2-azole)bis(bipyridyl)ruthenium(II) complexes: electrochemistry, luminescent properties, and electro- and photocatalysts for CO_2 reduction *Inorg. Chem*. **2021**, *60* (2), 692-704.

19. Aresta, M.; Nobile, C. F.; Albano, V. G.; Forni, E.; Manassero, M., New nickel–carbon dioxide complex: synthesis, properties, and crystallographic characterization of (carbon dioxide)-bis(tricyclohexylphosphine)nickel. *J. Chem. Soc., Chem. Comm.* **1975,** (15), 636-637.

20. Bhugun, I.; Lexa, D.; Saveant, J.-M., Ultraefficient selective homogeneous catalysis of the electrochemical reduction of carbon dioxide by an iron(0) porphyrin associated with a weak Broensted acid cocatalyst. *J. Am. Chem. Soc.* **1994,** *116* (11), 5015-16.

21. Bhugun, I.; Lexa, D.; Saveant, J.-M., Catalysis of the Electrochemical Reduction of Carbon Dioxide by Iron(0) Porphyrins: Synergistic Effect of Weak Broensted Acids. *J. Am. Chem. Soc.* **1996,** *118* (7), 1769-76.

22. Hawecker, J.; Lehn, J.-M.; Ziessel, R., Efficient photochemical reduction of CO2 to CO by visible light irradiation of systems containing $Re(bipy)(CO)_3X$ or $Ru(bipy)_3^{2+}$-Co^{2+} combinations as homogeneous catalysts. *J. Chem. Soc., Chem. Comm.* **1983,** (9), 536-538.

23. Sullivan, B. P.; Bolinger, C. M.; Conrad, D.; Vining, W. J.; Meyer, T. J., One- and two-electron pathways in the electrocatalytic reduction of CO_2 by fac-$Re(bpy)(CO)_3Cl$ (bpy = 2,2[prime or minute]-bipyridine). *J. Chem. Soc., Chem. Comm.* **1985,** (20), 1414-1416.

24. Hawecker, J.; Lehn, J.-M.; Ziessel, R., Electrocatalytic reduction of carbon dioxide mediated by $Re(bipy)(CO)_3Cl$ (bipy = 2,2′-bipyridine). *J. Chem. Soc., Chem. Comm.* **1984,** (6), 328-330.

25. Hawecker, J.; Lehn, J.-M.; Ziessel, R., Photochemical and Electrochemical Reduction of Carbon Dioxide to Carbon Monoxide Mediated by (2,2′-Bipyridine)tricarbonylchlororhenium(I) and Related Complexes as Homogeneous Catalysts. *Helv. Chim. Acta* **1986,** *69* (8), 1990-2012.

26. Costentin, C.; Drouet, S.; Robert, M.; Saveant, J.-M., A Local Proton Source Enhances CO_2 Electroreduction to CO by a Molecular Fe Catalyst. *Science* **2012,** *338* (6103), 90-94.

27. Costentin, C.; Robert, M.; Saveant, J.-M., Catalysis of the electrochemical reduction of carbon dioxide. *Chem. Soc. Rev.* **2013,** *42* (6), 2423-2436.

28. Riplinger, C.; Sampson, M. D.; Ritzmann, A. M.; Kubiak, C. P.; Carter, E. A., Mechanistic Contrasts between Manganese and Rhenium Bipyridine Electrocatalysts for the Reduction of Carbon Dioxide. *J. Am. Chem. Soc.* **2014,** *136* (46), 16285-16298.

29. Sung, S.; Li, X.; Wolf, L. M.; Meeder, J. R.; Bhuvanesh, N. S.; Grice, K. A.; Panetier, J. A.; Nippe, M., Synergistic Effects of Imidazolium-Functionalization on fac-Mn(CO)3 Bipyridine Catalyst Platforms for Electrocatalytic Carbon Dioxide Reduction. *J. Am. Chem. Soc.* **2019,** *141* (16), 6569-6582.

30. Nichols, E. M.; Derrick, J. S.; Nistanaki, S. K.; Smith, P. T.; Chang, C. J., Positional effects of second-sphere amide pendants on electrochemical CO_2 reduction catalyzed by iron porphyrins. *Chem. Sci.* **2018,** *9*, 2952.

31. Costentin, C.; Robert, M.; Savéant, J. M.; Tatin, A., Efficient and selective molecular catalyst for the CO_2-to-CO electrochemical conversion in water. *Proc. Natl. Acad. Sci. U. S. A.* **2015,** *112*, 6882.

32. Chapovetsky, A.; Do, T. H.; Haiges, R.; Takase, M. K.; Marinescu, S. C., Proton-Assisted Reduction of CO_2 by Cobalt Aminopyridine Macrocycles. *J. Am. Chem. Soc.* **2016,** *138*, 5765.

33. Sinha, S.; Sonea, A.; Shen, W.; Hanson, S. S.; Warren, J. J., Heterogeneous Aqueous CO_2 Reduction Using a Pyrene-Modified Rhenium(I) Diimine Complex. *Inorg. Chem.* **2019,** *58* (16), 10454-10461.

34. Schneider, T. W.; Ertem, M. Z.; Muckerman, J. T.; Angeles-Boza, A. M., Mechanism of Photocatalytic Reduction of CO2 by Re(bpy)(CO)3Cl from Differences in Carbon Isotope Discrimination. *ACS Catalysis* **2016**, 5473-5481.

35. Yang, G.; Zhang, W., Renaissance of pyridine-oxazolines as chiral ligands for asymmetric catalysis. *Chemical Society Reviews* **2018,** *47* (5), 1783-1810.

36. Nganga, J. K.; Samanamu, C. R.; Tanski, J. M.; Pacheco, C.; Saucedo, C.; Batista, V. S.; Grice, K. A.; Ertem, M. Z.; Angeles-Boza, A. M., Electrochemical Reduction of CO_2 Catalyzed by Re(pyridine-oxazoline)$(CO)_3$Cl Complexes. *Inorg. Chem.* **2017,** *56*, 3214-3226.

37. Stokes, B. J.; Opra, S. M.; Sigman, M. S., Palladium-catalyzed allylic cross-coupling reactions of primary and secondary homoallylic electrophiles. *J. Am. Chem. Soc.* **2012,** *134* (28), 11408-11.

38. Krejčik, M.; Daněk, M.; Hartl, F., Simple construction of an infrared optically transparent thin-layer electrochemical cell: Applications to the redox reactions of ferrocene, $Mn_2(CO)_{10}$ and $Mn(CO)_3$(3,5-di-t-butyl-catecholate) *J. Electroanal. Chem. Interf. Electrochem.* **1991,** *317* (1), 179-187.

39. CrysAlisPro, Rigaku Oxford Diffraction version 171.39.33b, **2017**.

40. SCALE3 ABSPACK – A Rigaku Oxford Diffraction program for Absorption Corrections, Rigaku Oxford Diffraction, **2017**.

41. Sheldrick, G. M., SHELXT-Integrated Space-Group and Crystal-Structure Determination, *Acta Cryst.* **2015,** (A71), 3-8.

42. Sheldrick, G. M., Crystal structure refinement with SHELXL, *Acta Cryst.* **2015,** *C71*, 3-8.

43. Zhao, Y.; Truhlar, D. G., The M06 suite of density functionals for main group thermochemistry, thermochemical kinetics, noncovalent interactions, excited states, and transition elements: two new functionals and systematic testing of four M06-class functionals and 12 other functionals. *Theor. Chem. Acc.* **2008,** *120* (1), 215-241.

44. Marenich, A. V.; Cramer, C. J.; Truhlar, D. G., Universal solvation model based on solute electron density and on a continuum model of the solvent defined by the bulk dielectric constant and atomic surface tensions. *J Phys Chem B* **2009,** *113* (18), 6378-96.

45. Andrae, D.; Häußermann, U.; Dolg, M.; Stoll, H.; Preuß, H., Energy-adjustedab initio pseudopotentials for the second and third row transition elements. *Theor. Chim. Acta* **1990,** *77* (2), 123-141.

46. Hehre, W. J., *AB INITIO Molecular Orbital Theory*. Wiley: 1986.

47. Frisch, M. J.; Trucks, G. W.; Schlegel, H. B.; Scuseria, G. E.; Robb, M. A.; Cheeseman, J. R.; Scalmani, G.; Barone, V.; Mennucci, B.; Petersson, G. A.; Nakatsuji, H.; Caricato, M.; Li,

X.; Hratchian, H. P.; Izmaylov, A. F.; Bloino, J.; Zheng, G.; Sonnenberg, J. L.; Hada, M.; Ehara, M.; Toyota, K.; Fukuda, R.; Hasegawa, J.; Ishida, M.; Nakajima, T.; Honda, Y.; Kitao, O.; Nakai, H.; Vreven, T.; Montgomery Jr., J. A.; Peralta, J. E.; Ogliaro, F.; Bearpark, M. J.; Heyd, J.; Brothers, E. N.; Kudin, K. N.; Staroverov, V. N.; Kobayashi, R.; Normand, J.; Raghavachari, K.; Rendell, A. P.; Burant, J. C.; Iyengar, S. S.; Tomasi, J.; Cossi, M.; Rega, N.; Millam, N. J.; Klene, M.; Knox, J. E.; Cross, J. B.; Bakken, V.; Adamo, C.; Jaramillo, J.; Gomperts, R.; Stratmann, R. E.; Yazyev, O.; Austin, A. J.; Cammi, R.; Pomelli, C.; Ochterski, J. W.; Martin, R. L.; Morokuma, K.; Zakrzewski, V. G.; Voth, G. A.; Salvador, P.; Dannenberg, J. J.; Dapprich, S.; Daniels, A. D.; Farkas, Ö.; Foresman, J. B.; Ortiz, J. V.; Cioslowski, J.; Fox, D. J. *Gaussian 09*, Gaussian, Inc.: Wallingford, CT, USA, 2009.

48. Cramer, C. J., *Essentials of Computational Chemistry: Theories and Models*. Wiley: 2013.

49. Kelly, C. P.; Cramer, C. J.; Truhlar, D. G., Single-Ion Solvation Free Energies and the Normal Hydrogen Electrode Potential in Methanol, Acetonitrile, and Dimethyl Sulfoxide. *The J. Phys. Chem. B* **2007,** *111* (2), 408-422.

50. Keith, J. A.; Grice, K. A.; Kubiak, C. P.; Carter, E. A., Elucidation of the selectivity of proton-dependent electrocatalytic CO_2 reduction by fac-Re(bpy)$(CO)_3$Cl. *J Am Chem Soc* **2013,** *135* (42), 15823-9.

51. Kelly, C. P.; Cramer, C. J.; Truhlar, D. G., Aqueous Solvation Free Energies of Ions and Ion−Water Clusters Based on an Accurate Value for the Absolute Aqueous Solvation Free Energy of the Proton. *J. Phys. Chem. B* **2006,** *110* (32), 16066-16081.

52. Isse, A. A.; Gennaro, A., Absolute potential of the standard hydrogen electrode and the problem of interconversion of potentials in different solvents. *J Phys Chem B* **2010,** *114* (23), 7894-9.

53. Sinha, S.; Berdichevsky, E. K.; Warren, J. J., Electrocatalytic CO_2 reduction using rhenium(I) complexes with modified 2-(2-pyridyl)imidazole ligands. *Inorg. Chim. Acta* **2016**, *460*, 63-68.

54. Morimoto, T.; Nakajima, T.; Sawa, S.; Nakanishi, R.; Imori, D.; Ishitani, O., CO_2 Capture by a Rhenium(I) Complex with the Aid of Triethanolamine. *J. Am. Chem. Soc.* **2013,** *135* (45), 16825-16828.

55. Appel, A. M.; Helm, M. L., Determining the Overpotential for a Molecular Electrocatalyst. *ACS Catalysis* **2014,** *4* (2), 630-633.

56. Pegis, M. L.; Roberts, J. A. S.; Wasylenko, D. J.; Mader, E. A.; Appel, A. M.; Mayer, J. M., Standard Reduction Potentials for Oxygen and Carbon Dioxide Couples in Acetonitrile and N,N-Dimethylformamide. *Inorg. Chem.* **2015,** *54* (24), 11883-11888.

57. Christensen, P.; Hamnett, A.; Muir, A. V. G.; Timney, J. A., An in situ infrared study of CO_2 reduction catalysed by rhenium tricarbonyl bipyridyl derivatives. *J. Chem. Soc., Dalton Trans.* **1992,** (9), 1455-1463.

58. Stor, G. J.; Hartl, F.; van Outersterp, J. W. M.; Stufkens, D. J., Spectroelectrochemical (IR, UV/Vis) Determination of the Reduction Pathways for a Series of $[Re(CO)_3(\alpha\text{-diimine})L']^{0/+}$ (L' = Halide, OTf-, THF, MeCN, n-PrCN, PPh_3, $P(OMe)_3$) Complexes. *Organometallics* **1995,** *14* (3), 1115-1131.

59. Johnson, F. P. A.; George, M. W.; Hartl, F.; Turner, J. J., Electrocatalytic Reduction of CO2 Using the Complexes $[Re(bpy)(CO)_3L]n$ (n = +1, L = $P(OEt)_3$, CH_3CN; n = 0, L = Cl^-, OTf^-

; bpy = 2,2-Bipyridine; OTf^- = CF_3SO_3) as Catalyst Precursors: Infrared Spectroelectrochemical Investigation. *Organometallics* **1996,** *15* (15), 3374-3387.

60. Smieja, J. M.; Kubiak, C. P., Re(bipy-tBu)(CO)3Cl-improved Catalytic Activity for Reduction of Carbon Dioxide: IR-Spectroelectrochemical and Mechanistic Studies. *Inorg. Chem.* **2010,** *49* (20), 9283-9289.

61. Smieja, J. M.; Sampson, M. D.; Grice, K. A.; Benson, E. E.; Froehlich, J. D.; Kubiak, C. P., Manganese as a Substitute for Rhenium in CO2 Reduction Catalysts: The Importance of Acids. *Inorg. Chem.* **2013,** *52* (5), 2484-2491.

62. Sampson, M. D.; Nguyen, A. D.; Grice, K. A.; Moore, C. E.; Rheingold, A. L.; Kubiak, C. P., Manganese catalysts with bulky bipyridine ligands for the electrocatalytic reduction of carbon dioxide: Eliminating dimerization and altering catalysis. *J. Am. Chem. Soc.* **2014,** *136* (14), 5460-5471.

63. Zeng, Q.; Tory, J.; Hartl, F. í., Electrocatalytic Reduction of Carbon Dioxide with a Manganese(I) Tricarbonyl Complex Containing a Nonaromatic α-Diimine Ligand. *Organometallics* **2014,** *33* (18), 5002-5008.

64. Machan, C. W.; Sampson, M. D.; Chabolla, S. A.; Dang, T.; Kubiak, C. P., Developing a Mechanistic Understanding of Molecular Electrocatalysts for CO_2 Reduction using Infrared Spectroelectrochemistry. *Organometallics* **2014,** *33* (18), 4550-4559.

65. Konno, H.; Kobayashi, A.; Sakamoto, K.; Fagalde, F.; Katz, N. E.; Saitoh, H.; Ishitani, O., Synthesis and properties of $[Ru(tpy)(4,4'\text{-}X_2bpy)H]^+$ (tpy=2,2′:6′,2″-terpyridine, bpy=2,2′-bipyridine, X=H and MeO), and their reactions with CO_2. *Inorg. Chim. Acta* **2000,** *299* (2), 155-163.

66. Garg, K.; Matsubara, Y.; Ertem, M. Z.; Lewandowska-Andralojc, A.; Sato, S.; Szalda, D. J.; Muckerman, J. T.; Fujita, E., Striking Differences in Properties of Geometric Isomers of [Ir(tpy)(ppy)H]+: Experimental and Computational Studies of their Hydricities, Interaction with CO2, and Photochemistry. *Angew. Chem. Int. Ed.* **2015,** *54* (47), 14128-14132.

67. Schneider, T. W.; Hren, M. T.; Ertem, M. Z.; Angeles-Boza, A. M., $[Ru^{II}(tpy)(bpy)Cl]^{+}$-Catalyzed reduction of carbon dioxide. Mechanistic insights by carbon-13 kinetic isotope effects. *Chem. Comm.* **2018,** *54* (61), 8518-8521.

68. Ishida, H.; Tanaka, K.; Morimoto, M.; Tanaka, T., Isolation of intermediates in the water gas shift reactions catalyzed by $[Ru(bpy)_2(CO)Cl]^{+}$ and $[Ru(bpy)_2(CO)_2]^{2+}$. *Organometallics* **1986,** *5* (4), 724-730.

69. Hirotaka Nagao, T. M., Koji Tanaka, Carbon-Carbon Bond Formation in Multi-electron Reduction of Carbon Dioxide Catalyzed by $[Ru(bpy)(trpy)(CO)]^{2+}$ (bpy = 2,2′-bipyridine; trpy = 2,2′:6′,2″-terpyridine). *Chem. Lett.* **1993,** *22* (6), 955-958.

70. Rao, H.; Lim, C.-H.; Bonin, J.; Miyake, G. M.; Robert, M., Visible-Light-Driven Conversion of CO_2 to CH_4 with an Organic Sensitizer and an Iron Porphyrin Catalyst. *J. Am. Chem. Soc.* **2018,** *140* (51), 17830-17834.

71. Rao, H.; Schmidt, L. C.; Bonin, J.; Robert, M., Visible-light-driven methane formation from CO_2 with a molecular iron catalyst. *Nature* **2017,** *548* (7665), 74-77.

72. Shirley, H.; Su, X.; Sanjanwala, H.; Talukdar, K.; Jurss, J. W.; Delcamp, J. H., Durable Solar-Powered Systems with Ni-Catalysts for Conversion of CO_2 or CO to CH_4. *J. Am. Chem. Soc.* **2019,** *141* (16), 6617-6622.

73. Schneider, T. W.; Ertem, M. Z.; Muckerman, J. T.; Angeles-Boza, A. M., Mechanism of Photocatalytic Reduction of CO_2 by $Re(bpy)(CO)_3Cl$ from Differences in Carbon Isotope Discrimination. *ACS Catalysis* **2016,** *6* (8), 5473-5481.

For Table of Contents Only

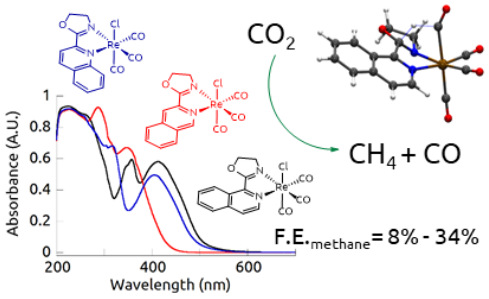

SYNOPSIS

Three rhenium tricarbonyl complexes containing (iso)quinoline-oxazoline ligands were synthesized, structurally and electrochemically characterized, and screened for CO_2 reduction activity. The electrocatalytic reduction of CO_2 by these complexes produce CO and CH_4. Density functional theory (DFT) calculations support a ligand-assisted activation of the substrate.